arXiv Hep-Ph Citation Network Analysis

Contents

1. Introduction
2. Dataset Analysis and Preprocessing
3. Exploratory Graph Analysis
4. Community Detection
    1. Louvain
    2. Label Propagation
5. Temporal Community Detection
6. Summary and Takeaways
7. Source Code
8. References

Introduction

This report details my analysis of the arXiv Hep-Ph Citation Network [1] as my submission for the Precog Recruitment Task (2024) . I have completed both the Exploratory Graph Analysis as well as the implementation of community detection algorithms and Temporal Community Analysis. The bonus task was not attempted due to time constraints

I set out with the aim of analyzing the dataset, implementing and running varying community detection algorithms on the network, and finally conducting a temporal analysis of the network. To accomplish this task, we shall first implement the Louvain and Label Propagation community detection algorithms for static community detection. Then we shall perform temporal community detection by dividing the graph into snapshots, where each such snapshot is a subset of the network and contains all edges and nodes occurring before a date t in the dataset. We will use conductance to measure community quality over time and we shall use various plots to compare Louvain and Label Propagation over time and compare them to other SOTA algorithms.

We will also use the arXiv API to analyze the results of different community detection algorithms and see if they actually are providing communities with papers involving similar fields of research.

We hypothesize that Louvain will generate large higher quality communities than Label Propagation as the Louvain algorithm, and it's currently used predecessor the Leiden algorithm, are widely used in the field of community detection as well as citation network analysis. We also hypothesize that the conductance will decrease over time, indicating that the community boundaries strengthen as they become more focused on their sub-field within the Hep-Ph field.

Our choice of tool for analysis will be graph-tool [2], an extremely fast and easy to use python library for network analysis. We initially use NetworkX for some preprocessing tasks.

Dataset Analysis and Preprocessing

The dataset is available at [1]. There are 2 files, in this dataset - one containing an edge list and another containing the date of publication of each node in the dataset.

After some analysis of the dataset, we notice that there may be some issues with the following,

- There are self loops in the dataset - This makes no sense as a paper cannot cite itself.
- Papers have more than one date of publication - This most likely indicates that the paper has been updated.

- There are edges going from a older paper to a newer paper - This makes no sense as a paper cannot cite a paper in the future.
- Some papers do not have dates associated with them.
- Papers cite each other on the same date - This may be indicative of papers being published in the same conference/publication and have cited each others work.
- There is a large component and several small components, all of which contain a single node with no edges to other nodes.

We do the following to correct the above issues in order to proceed with our analysis

1. We remove all self-loops.
2. If there is more than one date of publication, we take the last provided date of a paper to be its date of publication.
3. We remove all edges contradicting the flow of time. (i.e. pointing from an older paper to a newer one)
4. We remove cyclic citations by using the preprint transformation [3]. There were only 48 2-cycles and 2 3-cycles present, as would be expected due to the rarity of cyclic citations.
5. After all of the above, we select the largest weakly connected component.

Finally, after the above we are left with $30,438$ nodes and $345,573$ edges. Our results are validated by that of [4]. Our final node and edge counts are different due to use using the preprint transformation.

Exploratory Graph Analysis

We first plot the number of nodes per year and the number of edges per year.

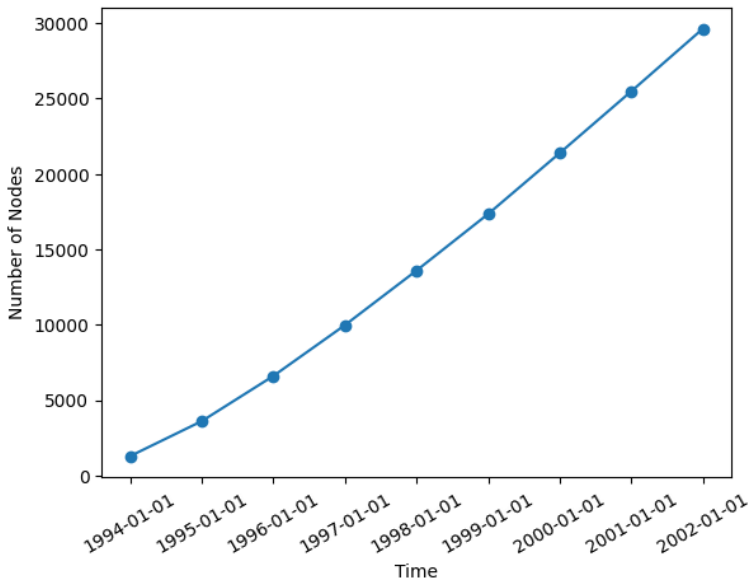

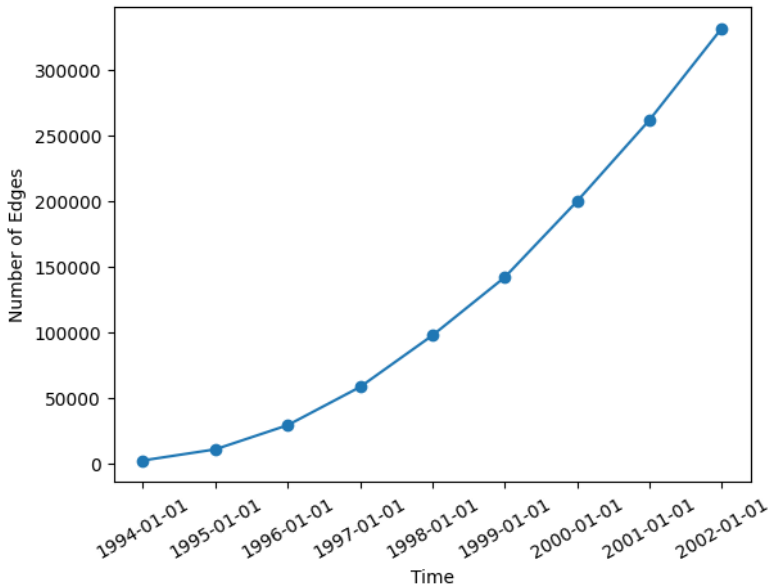

As we can see, the number of nodes and edges are increasing super linearly, with the number of edges more so than the number of nodes. This tells us that recent papers have, on average, a larger number of citations than previous papers. This will be more clear when we plot the in and out degree distributions of nodes.

Now we plot the *Densification Power Law plot* [5], which is simply the log-log plot of number of edges $e(t)$ versus the number of nodes $n(t)$.

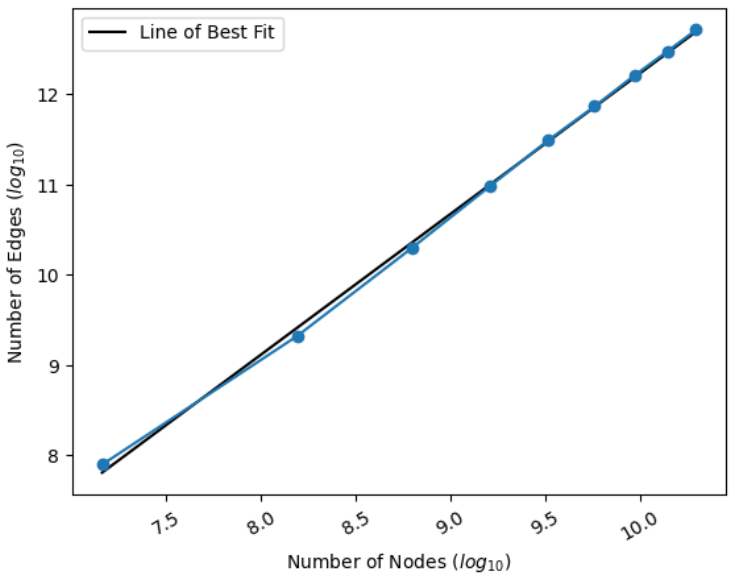

As we can see, the plot is almost linear, and the line of best fit has a positive slope of $a = 1.558$ (which is validated by [5] and once again shows that our preprocessing was valid). As per [5], this is similar in other real world graphs as they tend to get denser and more connected over time, which is what we see in this case as well.

We now plot the global clustering coefficient of the graph against time. The global clustering coefficient of a graph is defined as,

$$C = \frac{\text{Number of closed triplets}}{\text{Number of triplets}}$$

where a closed triplet is a group of 3 nodes joined by 2 edges and an open triplet is a group of 3 nodes joined by 3 edges (1 between each). The clustering coefficient of a graph is a measure of how much nodes in the graph tend to cluster together. According to studies, in real world networks, nodes create tightly knit groups, the likelihood of which is higher than when edges are randomly created between nodes.

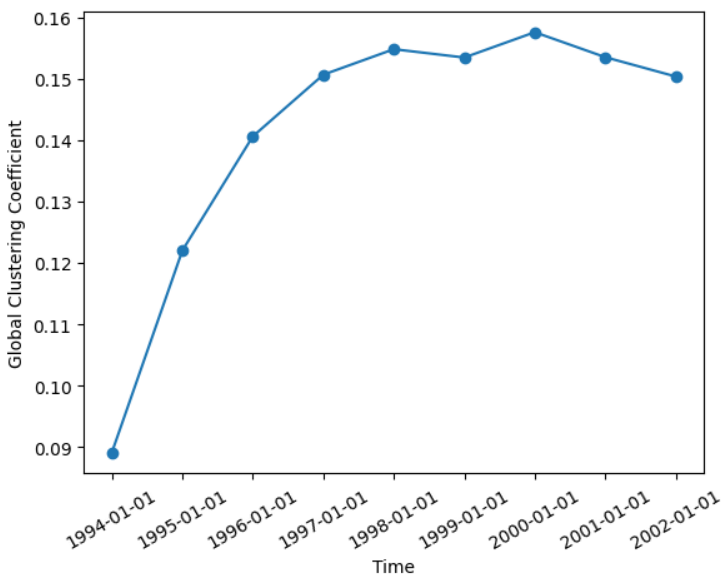

We see that the clustering coefficient of the graph increases with time and then remains mostly constant, indicating an increase in density over time after which the increase in clustering is offset by a large increase in nodes.

We now plot the pseudo-diameter of the graph over time. The pseudo-diameter is an approximation of the diameter, which is the size of the largest path in a graph. We use the pseudo-diameter here as it is infeasible to calculate the diameter of such a large graph quickly. We consider the edges to be undirected to calculate the diameter.

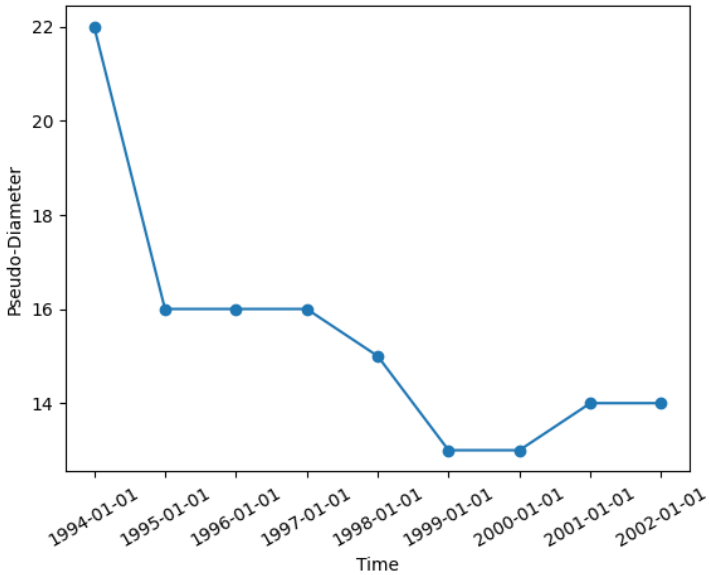

We see that the diameter decreases with time, indicating that newer nodes act as bridges that shorten the distance between older nodes.

We now plot the out degree and in degree histograms over time.

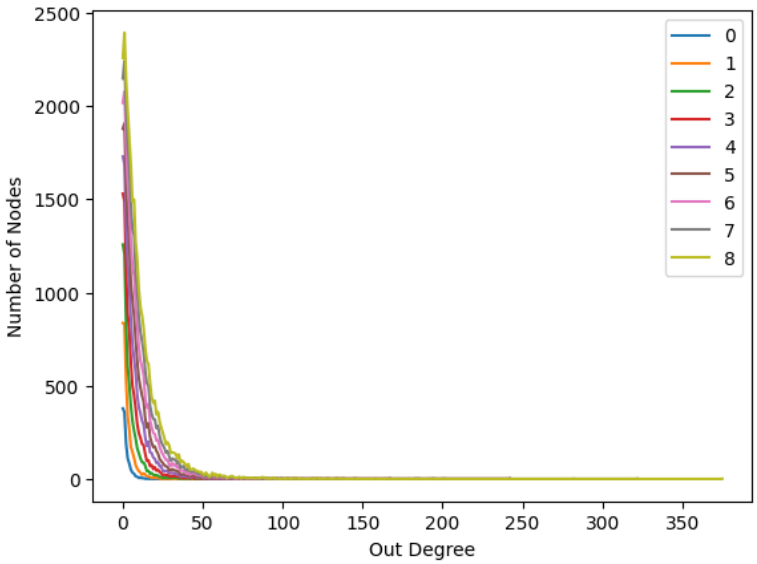

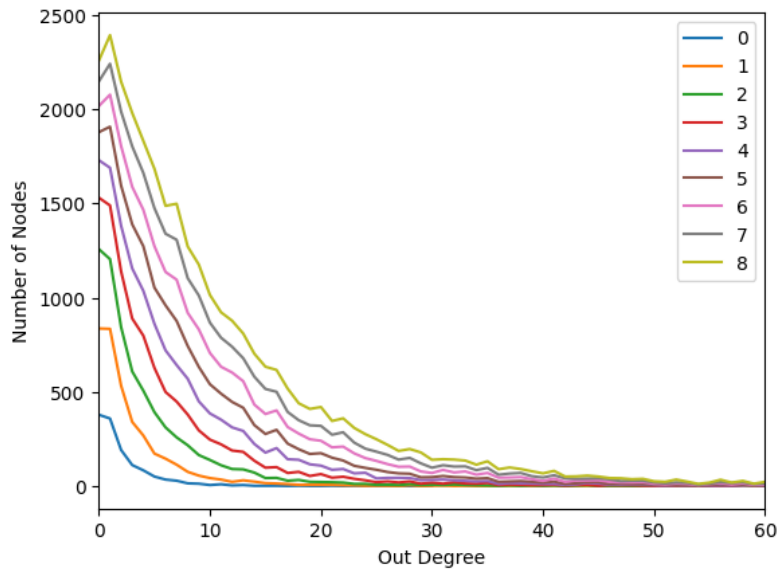

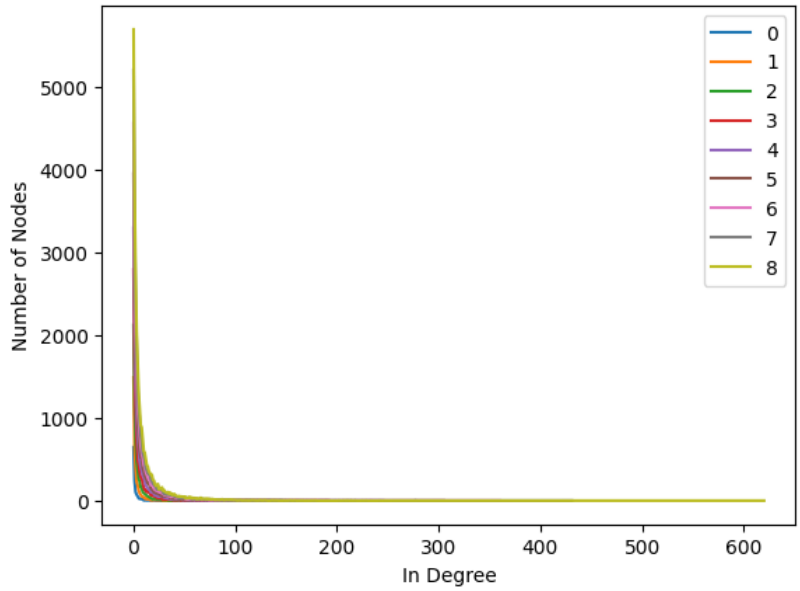

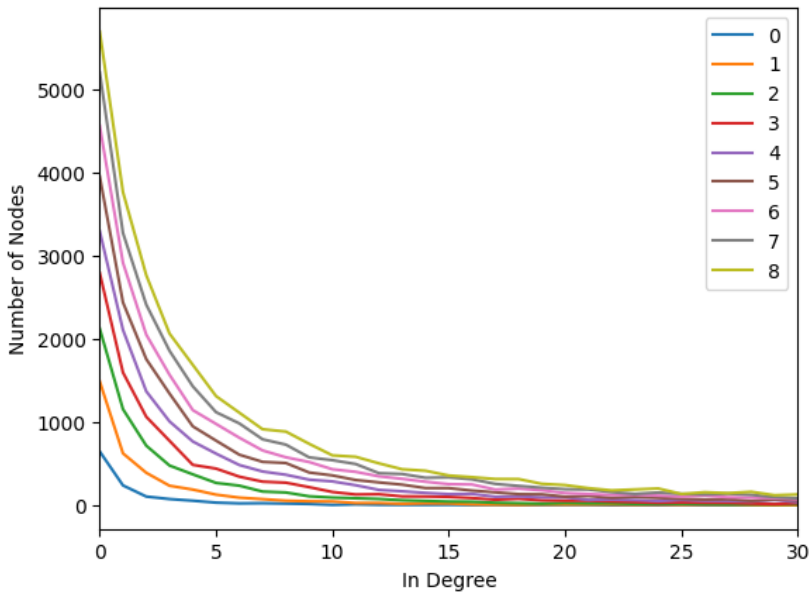

As we can see, the number of nodes with out degree between 1 and 30 greatly increases over time, indicating that newer papers tend to have higher number of citations. The number of

nodes with in degree between 1 and 15 also greatly increases over time, indicating that as time goes on, papers tend to get more citations, as one would expect.

We end this section with the assortativity plots of the graph w.r.t. in, out, and total degree over time. The assortativity of a graph measures the tendency of nodes with a similar property to preferentially form links with each other. We measure the assortativity w.r.t. the properties of in, out, and total degree.

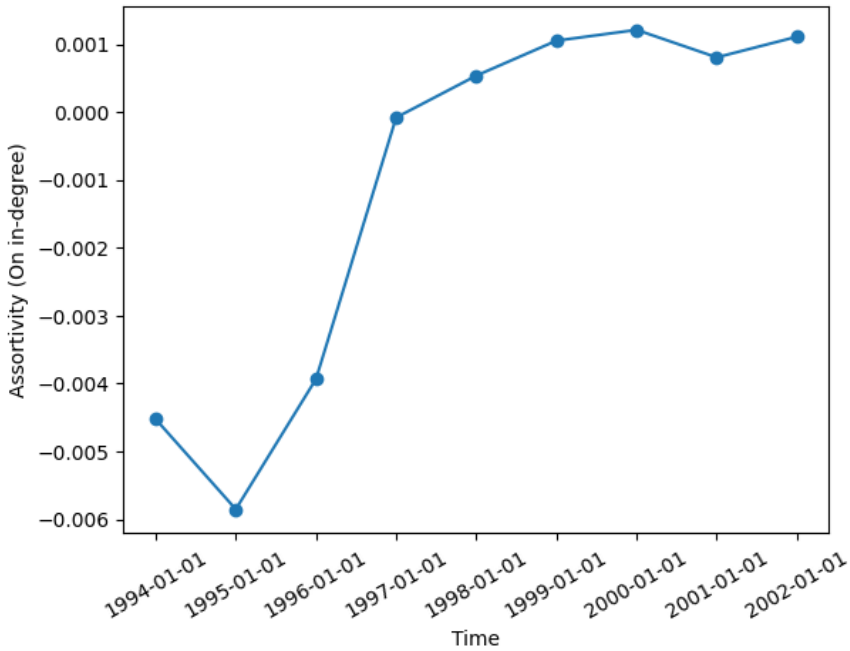

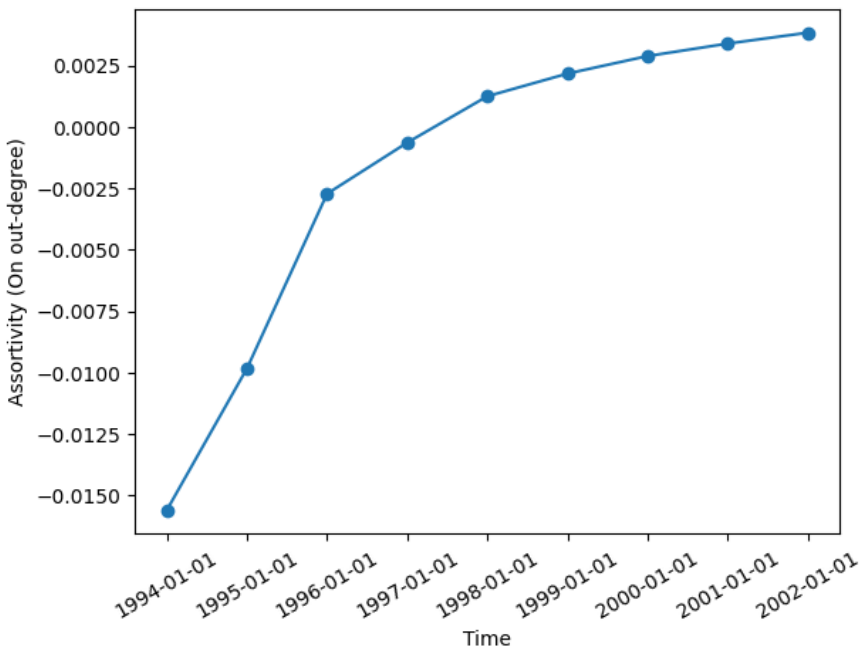

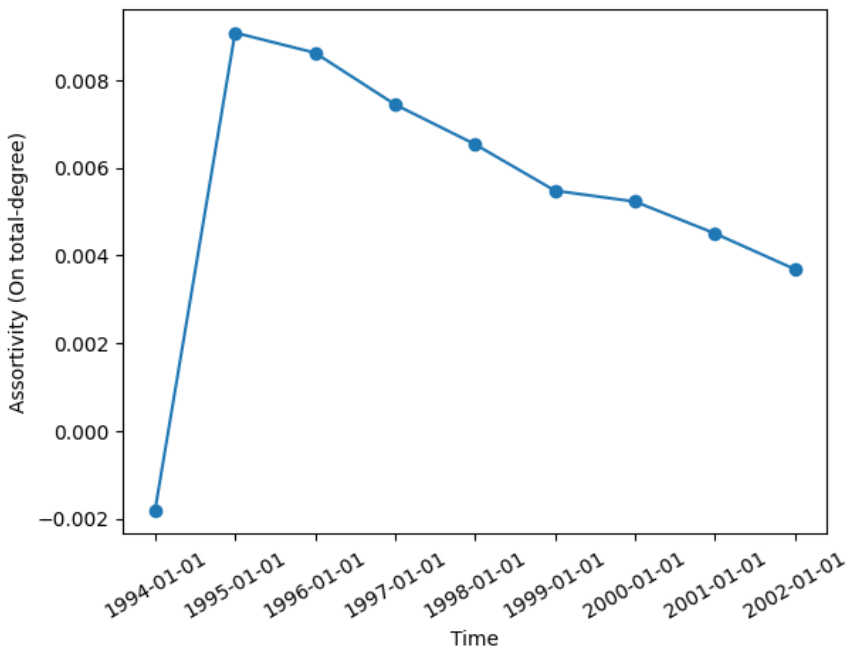

As we can see, for all three properties, the assortativity of the graph is around 0. This tells us that papers with higher citations do not tend to cite other papers with high citations and the same holds for papers with low citations. This is interesting as it shows that regardless of their citation count, papers still seem to be cited by newer papers indicating that most papers are cited regardless of their acceptance by the community (measured in terms of citation count).

Community Detection

To perform community detection, we implemented the Louvain and Label Propagation algorithms. Louvain is a popular and well excepted method of community detection and is used frequently in the field of citation analysis. Label Propagation is a slightly older algorithm which uses only the network structure to decide communities and runs in near linear time and does not maximize any heuristic. We chose these so as to ensure we perform analysis on the communities detected by both an algorithm which maximizes a heuristic and an algorithm which instead focuses on network structure.

Note that for community detection, we assumed each edge to be undirected.

The Louvain Algorithm

The Louvain algorithm is a highly popular community detection algorithm which maximizes a heuristic known as modularity. The modularity of a graph is defined as

$$Q = \frac{1}{2m} \sum_{i=1}^{N} \sum_{j=1}^{N} [A_{ij} - \frac{k_i k_j}{2m}] \delta(c_i, c_j)$$

where N is the number of nodes in the graph, A_{ij} is an entry in the graphs adjacency matrix, m is the sum of all edge weights in the graph, k_i and k_j are the sum of the weights of the edges incident on i and j respectively, c_i and c_j are the communities to which i and j belong to, and δ is the Kronecker delta

$$\delta(c_i, c_j) = \begin{cases} 1 & \text{if c}_i \text{ and c}_j \text{ belong to the same community} \\ 0 & \text{otheriwse} \end{cases}$$

The algorithm does the following

1. Place each node into their own community
2. For each node
    1. Check the change in modularity when adding the node to one of its neighboring communities.
    2. Choose the community for which the change in modularity is the maximum.
    3. If the change in modularity is positive, place the node in that community.
3. Repeat 2 until there is no change in community possible for any node that increases the modularity.
4. Now convert the graph into its condensation graph where each node is a community. Repeat 1 until each community is a single node.

However, this may take too long to end, so instead we stop running Louvain when the change in modularity before and after step 2 is less than 10^{-7}.

The speed of Louvain lies in the fact that it can use a trick to calculate the change in modularity without calculating the modularity for the entire graph and using that to calculate the change.

We derive the formula below. First consider the change in modularity when moving a node i from community D to C,

$$\Delta Q(D \to i \to C) = \Delta Q(D \to i) + \Delta Q(i \to c)$$

Now we derive $\Delta Q(i \to C)$. First, note that the modularity of the community C, can be defined as follows,

$$Q(C) \equiv \frac{\sum_{in,C}}{2m} - \left(\frac{\sum_{tot,C}}{2m}\right)^2$$

where $\sum_{in,C} \equiv \sum_{i,j \in C} A_{ij}$ and $\sum_{i \in C} k_i$.

Now, define

$$k_{i,C} \equiv \text{sum of link weights between node } i \text{ and nodes in C}$$

and define

$$k_i \equiv \text{sum of all link weights of node } i$$

Hence, before placing i in C,

$$Q_{before} = Q(C) + Q(\{i\})$$

and after placing i in C,

$$Q_{after} = Q(C + \{i\})$$

And,

$$\Delta Q(i \to C) = Q_{after} - Q_{before}$$

Which on solving we get,

$$\Delta Q(i \to C) = \frac{1}{m}\left(k_{i,C} - \frac{k_i \sum_{tot,C}}{2m}\right)$$

and similarly we can get,

$$\Delta Q(D \to i) = -\frac{1}{m}\left(k_{i,D} - \frac{k_i(\sum_{tot,D} - k_i)}{2m}\right)$$

We subtract k_i from $\sum_{tot,D}$ as we need to calculate the sum of all node degrees in D excluding that of i.

Hence,

$$\Delta Q(D \to i \to C) = \Delta Q(D \to i) + \Delta Q(i \to C)$$

and on solving we get,

$$\Delta Q(D \to i \to C) = \frac{k_i(\sum_{tot,D} - k_i - \sum_{tot,C}) + 2m(k_{in,C} - k_{in,D})}{2m^2}$$

However, the denominator here is always positive, and we only want to compare the ΔQ values and not actually use them, and hence we can remove the denominator and use just the

numerator. This also saves a costly division and improves accuracy as the numerator will always be whole numbers in our case (since we have no edge weights).

On running Louvain on our graph, we get the following results,

Community Index	Number of Nodes
0	2651
1	2752
2	3476
3	1974
4	3518
5	3374
6	4885
7	4305
8	3133
9	200
10	25
11	10
12	3
13	9
14	3
15	6
16	4
17	5
18	4
19	4

We also achieve a modularity of 0.6896 which is similar to results in [4], indicating that our implementation is working well. The small communities of size 4 are most likely those created by our pre-print transformation. As expected, Louvain creates large communities with good

interlinking between them, as can be seen below. Louvain chooses larger communities due to it's resolution limit, and is unable to detect well connected smaller communities.

Label Propagation

Label propagation is a simple and fast algorithm for community detection. We assign each node an initial label. Then, for each node, we look at its neighbors and decide on its new label based on which label is the most common amongst its neighbors (ties are broken randomly here). We then do the same repeatedly until each neighbor has a label which the majority of is neighbors has.

The algorithm does not produce the same results each time due to the randomness. On running Label Propagation on our graph, we get the following results,

Number of labels: 235

Community Index	Number of Nodes
0	582
1	268
2	21
3	8931
4	1781
5	1754
6	330
7	155
8	55
9	1433
10	638
11	793
12	1247
13	817
14	24
15	463
16	272
17	149
18	367
19	246
20	393
21	60
22	155
23	49
24	3
25	205
26	158
27	1100
28	106
29	33
30	42
31	8
32	15
33	131
34	109
35	515
36	27
37	402
38	137
39	92
40	16
41	22
42	67
43	19

44	224
45	1436
46	137

As we can see, there are far more communities detected by label propagation than by Louvain. Label propagation has detected 235 different communities, of varying sizes. The largest is a community of size 8931, larger than any of the Louvain communities. However, we have also obtained a large number of smaller communities. On plotting the edge counts between communities, we see the below, (note that communities have been relabeled in order of size)

and if we exclude the large community with over 100000 edges in it we see the following, (note that 0 here is not the same as the 0 above and is instead 1 as all the labels have been shifted by 1)

This shows us that Label Propagation can find both large well connected communities as well as smaller well connected communities, something that Louvain is not able to do so well in.

Temporal Community Detection

We now perform community detection on slices of the network. To ensure speed in getting the results and brevity in the analysis, we have chosen 2 month slices starting from 1995-06-01 and going till 2000-06-01. Larger time slices causes a large amount of nodes to be added, causing the temporal analysis to worsen.

The snapshot of the network at each time slice contains all nodes and edges present in the network before that date, hence ensuring the consecutive snapshots are super sets of the previous ones. The snapshot may not consist of a single weakly connected component, and in that case we select the largest weakly connected component. This does not cause any issues as for each snapshot, the largest weakly connected component is a super set of the largest weakly connected components of previous snapshots.

We then perform community detection on each snapshot using the Louvain Algorithm, Label Propagation, and by inferring a SBM (Stochastic Block Model). After this, we greedily assign communities in a newer snapshot labels from the prior snapshot by comparing the community sets using the Jaccard Similarity of the 2 community sets.

We first plot the number of communities over time

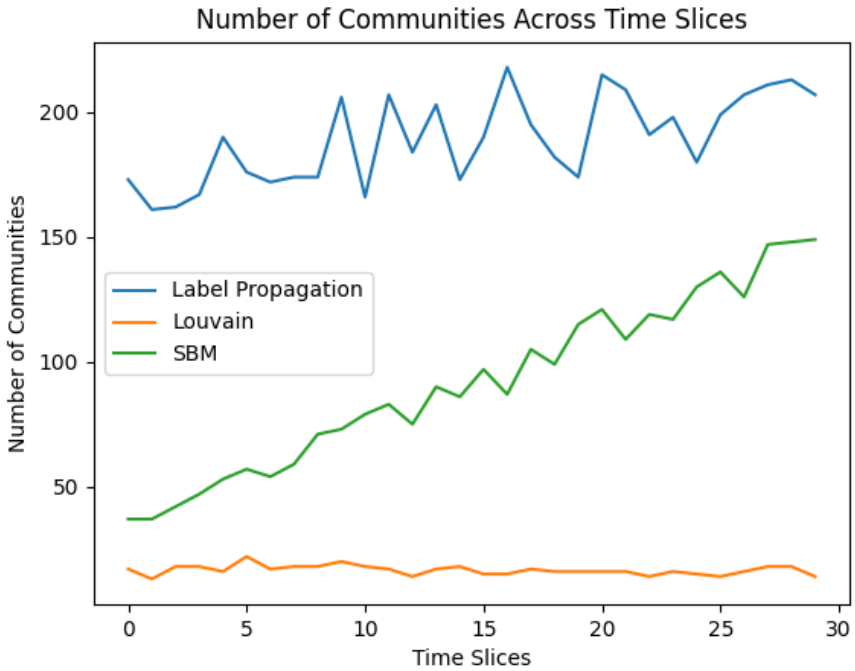

Louvain starts of with and continues to have a small number of communities. SBM has a steadily growing number of communities. Label Propagation has a large number of communities, and is slowly growing in number of communities. This shows that Louvain consistently finds the same large community and continues to grow that community, whereas Label Propagation tends to find several smaller sized communities.

We now plot community births and deaths over time,

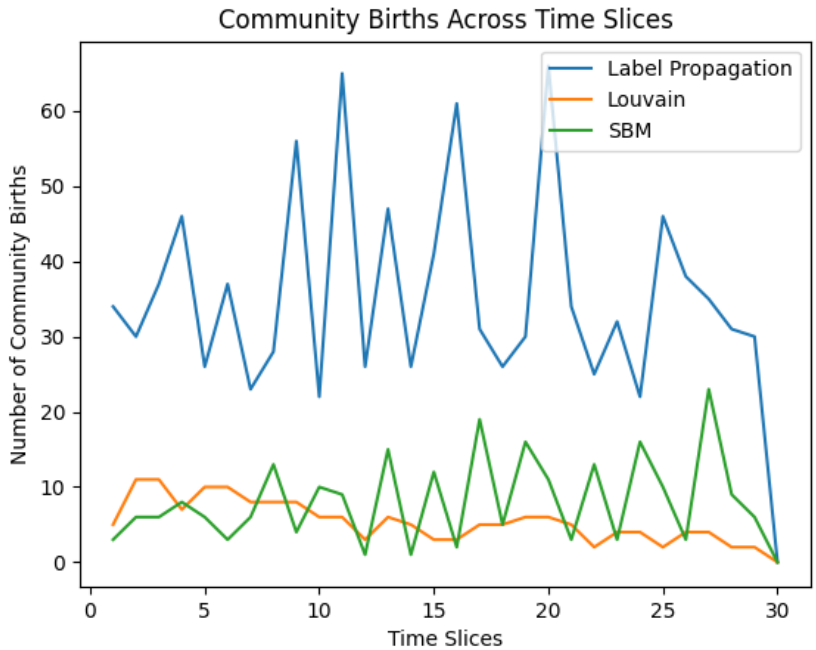

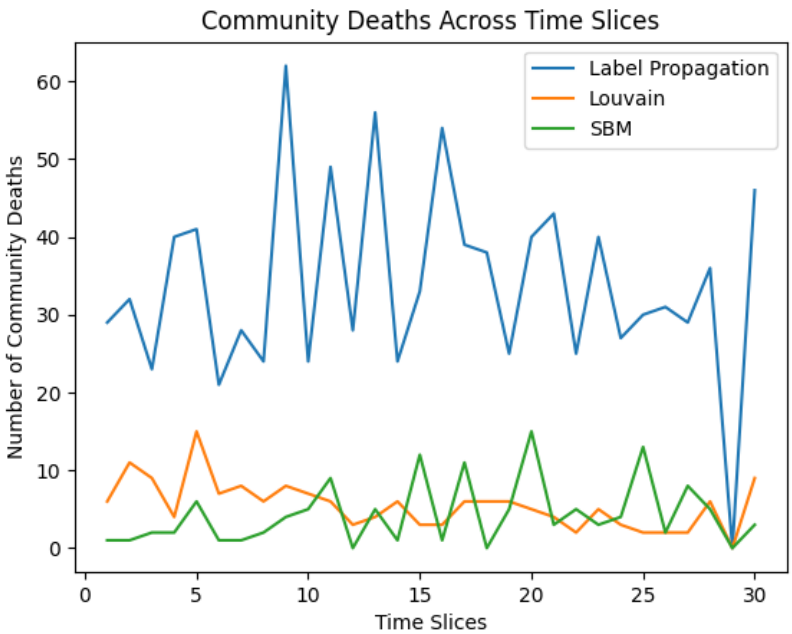

As we can see, Label Propagation continually has large numbers of community deaths and births, showcasing the non-determinism in its algorithm. Louvain and SBM have similar numbers of community deaths and births, but SBM has larger variance.

These plots are quite generic and do not provide us much information with regards to the quality of the temporal communities generated. The following plots will aid us with this.

We now plot the age of a community (defined as the number of consecutive time slices from its birth to its death) vs. the average size of a community over its lifetime.

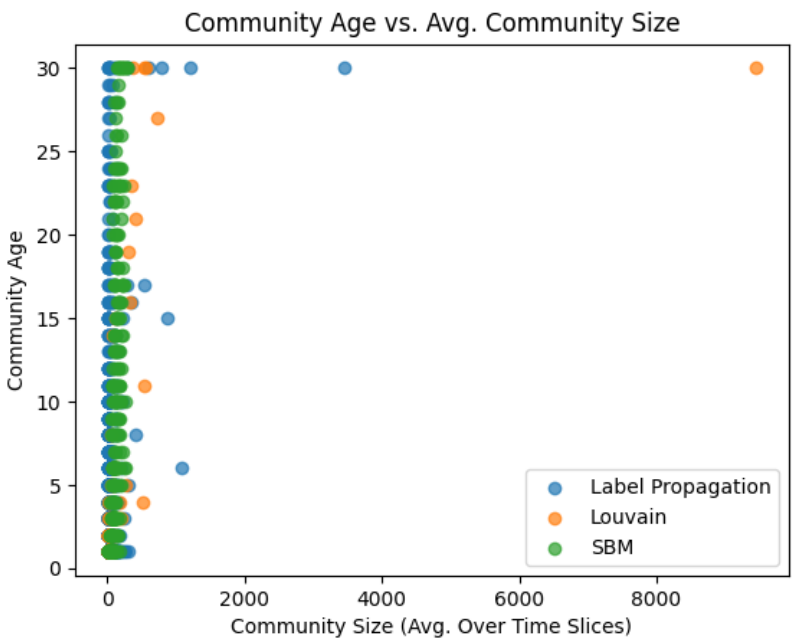

As we can see, there are a few long living Louvain communities, most larger than communities produced by the other algorithms except for one massive community which is much larger than

all other communities and has survived through all 31 time slices. There also a few large Label Propagation communities, and all of the SBM communities are quite small. However, we can infer some more information by zooming in on the smaller communities.

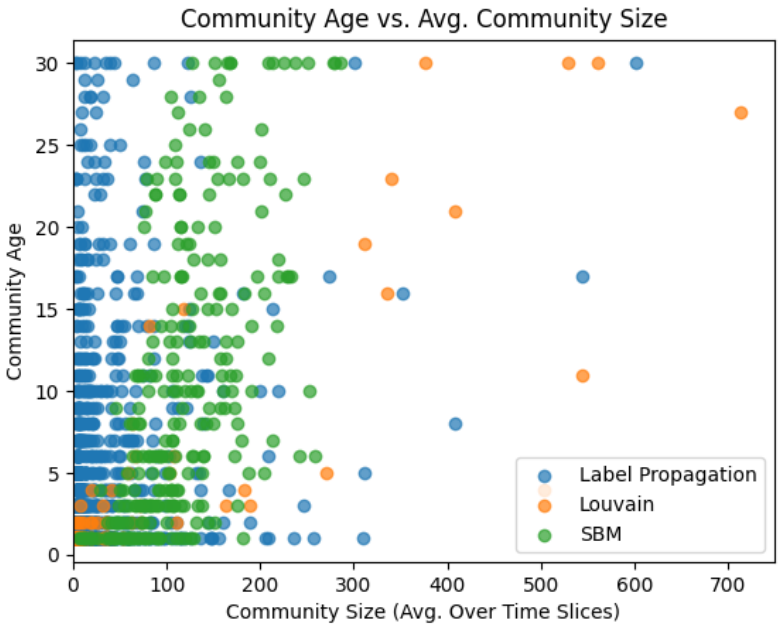

As we can see, Louvain has few long lived communities, with most of its communities dying out in under 5 time slices. Label Propagation and SBM however have a spread of communities over all ages, with the bulk of communities found by label propagation extremely small in size, in comparison to the SBM communities, almost all of which are medium in size, and on average, larger than the Label Propagation communities.

We also plot the community age vs. standard deviation in community size below, indicating that almost all SBM communities have jumps in their size of about half their average size. All the Louvain communities have high standard deviations, indicating large arrivals and departures of nodes from the communities. Large and medium sized Label Propagation communities also have high standard deviations.

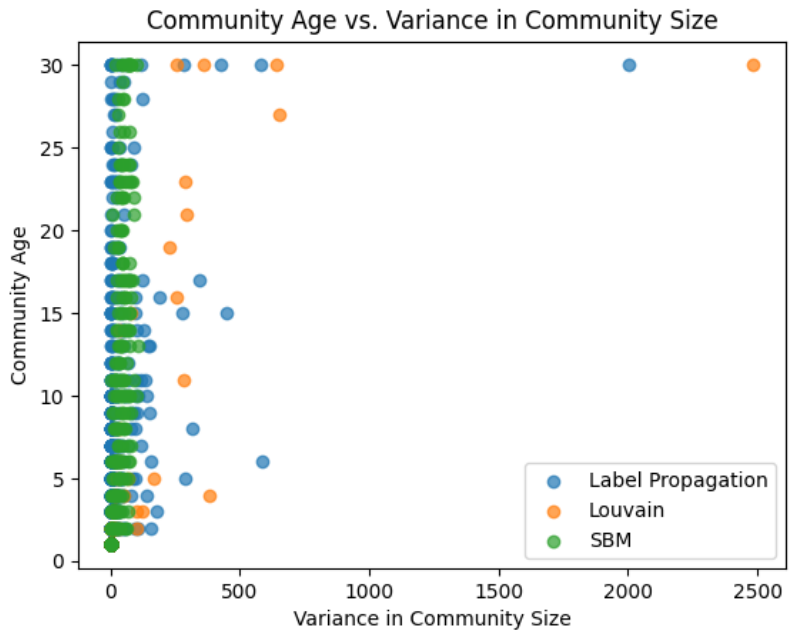

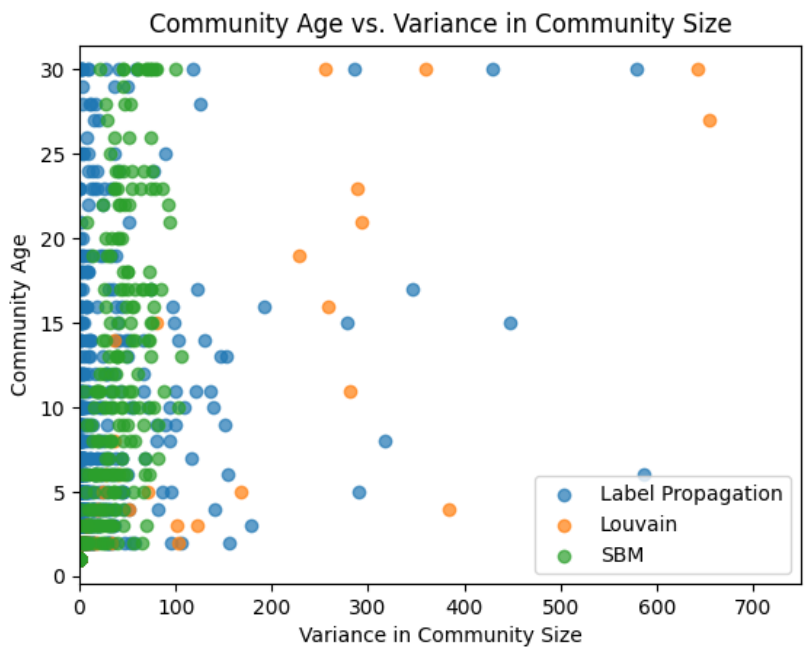

To get further insight into the quality of these communities, we define the **consistent size** of a community to be the size of the largest common subset across the lifetime of a community. Now if we plot age vs. consistent size of a community, we see the following,

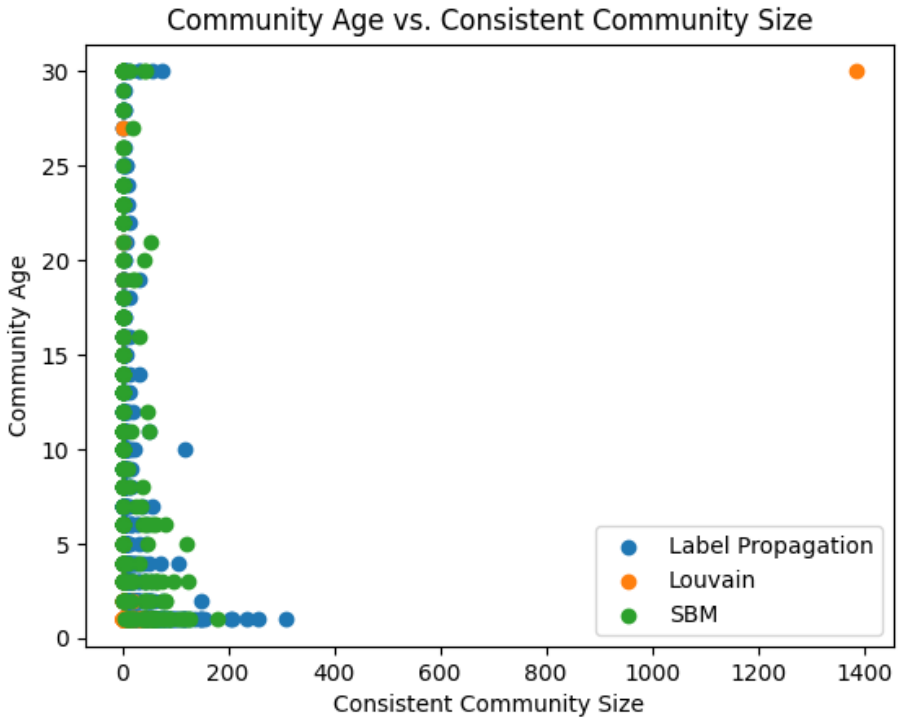

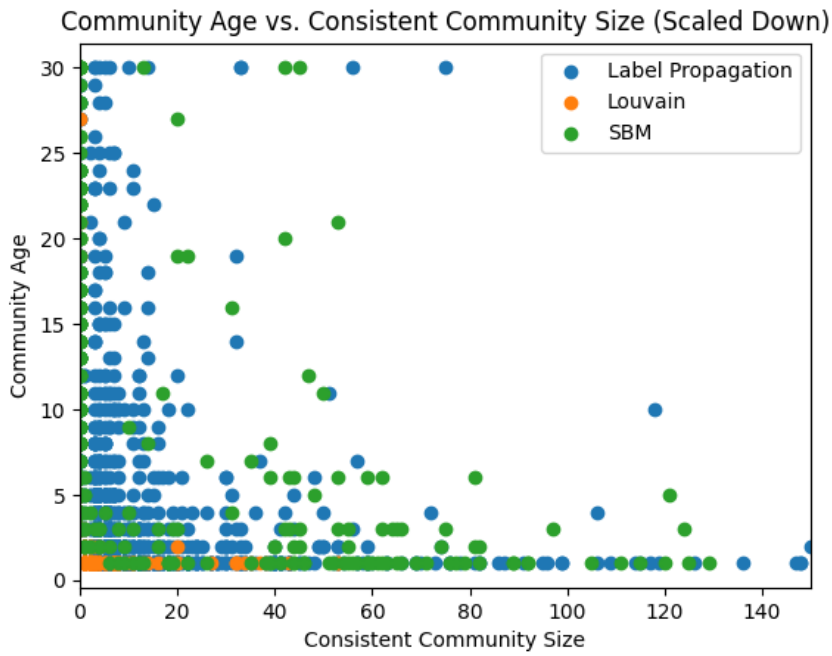

The large Louvain community has a large consistent size and still holds its place as the largest community, but as we zoom into the communities with smaller consistent size, we see that the small Label Propagation communities mostly retain all their elements whereas most of the SBM communities do not retain all of their elements and only a few of the medium sized SBM communities retain elements. This shows us that label propagation works well on small communities, and is consistently being able to detect them and SBM works ok on medium communities, and consistently detects some of them, whereas Louvain is good at detecting large communities and consistently detects them.

Below we plot the size of the communities with largest consistent size over time. As we can see, the largest label propagation community is the most consistent one, and other large label propagation communities are the others. The SBM communities are medium sized and stay mostly constant in their community size. The Louvain community increases in size almost linearly, before plateauing.

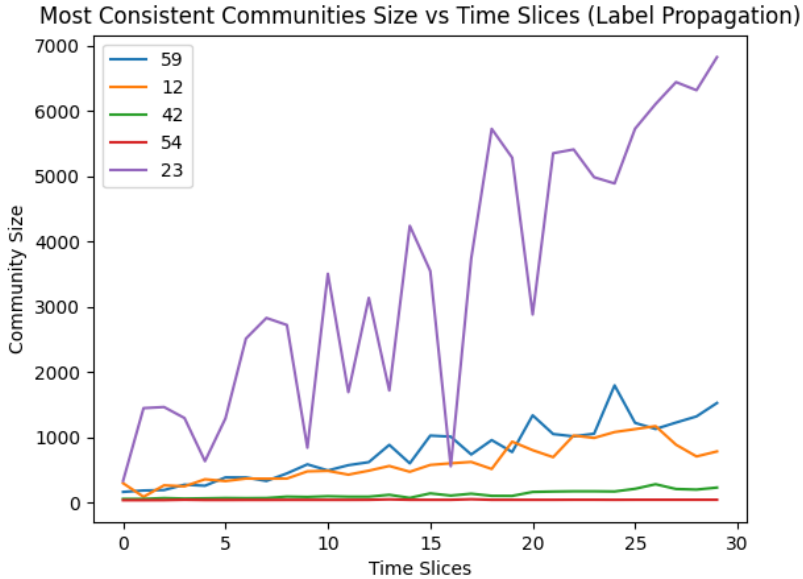

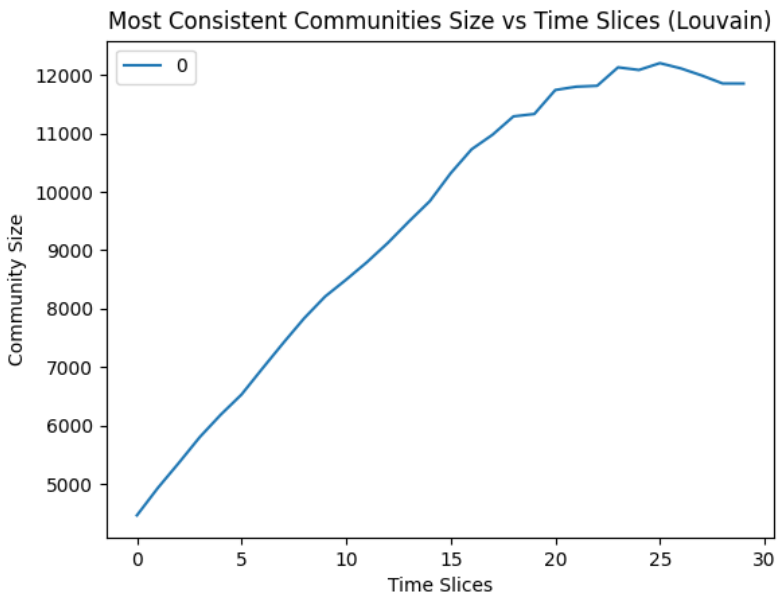

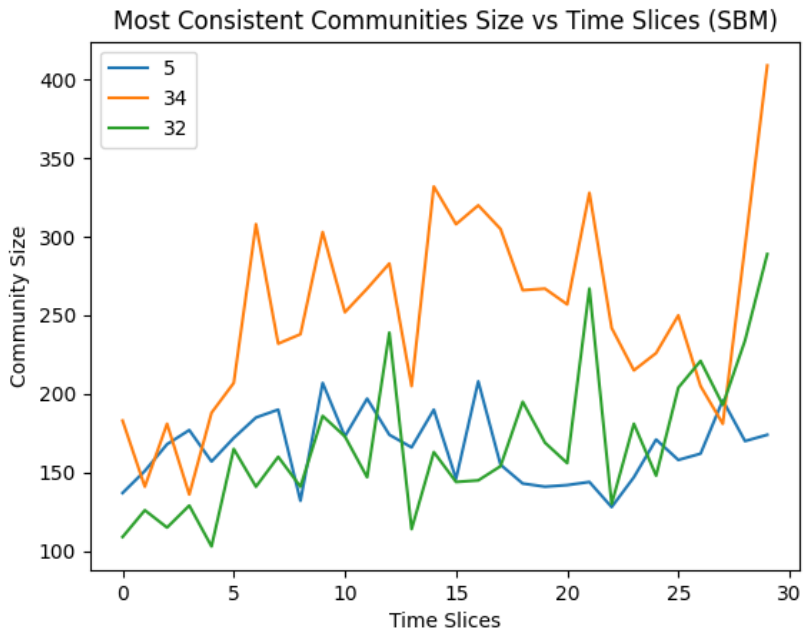

We also plot the conductance of these consistent communities below. As we can see, the conductance values for Label Propagation are mostly low and constant, albeit some having high variance, thus indicating good community structure. For Louvain, the conductance continually decreases, indicating an initial low quality community which was refined over time. For SBM, the values start off low, increase somewhat and then plateau once again, indicating slightly worsened community structure than when starting. However, the final conductance values are also quite low, indicating good community structure.

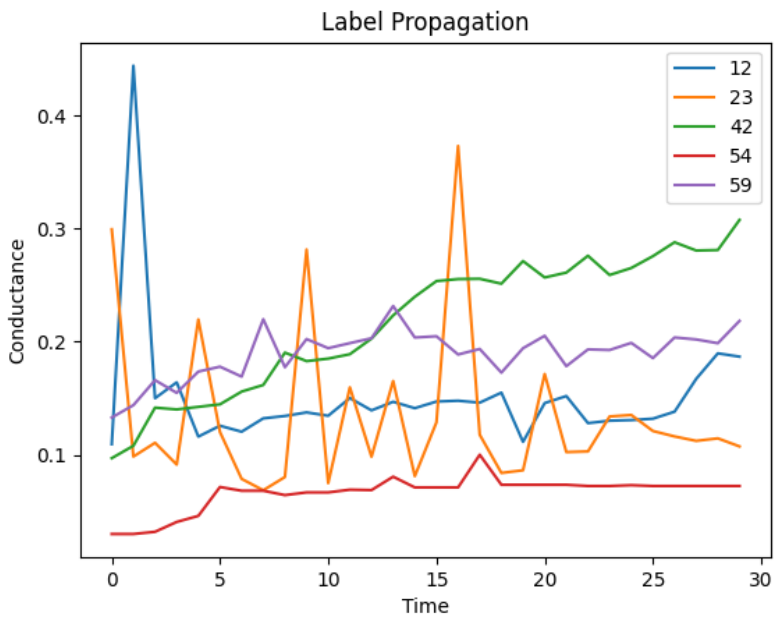

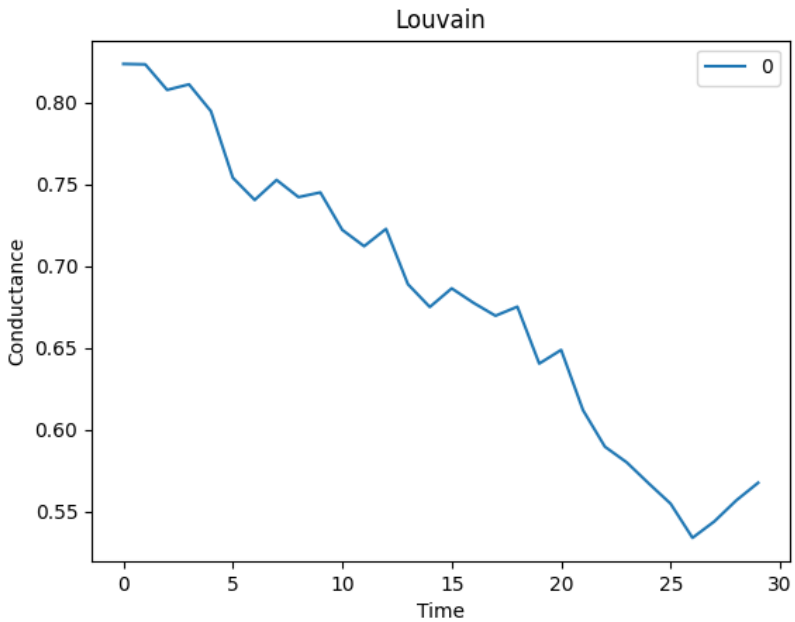

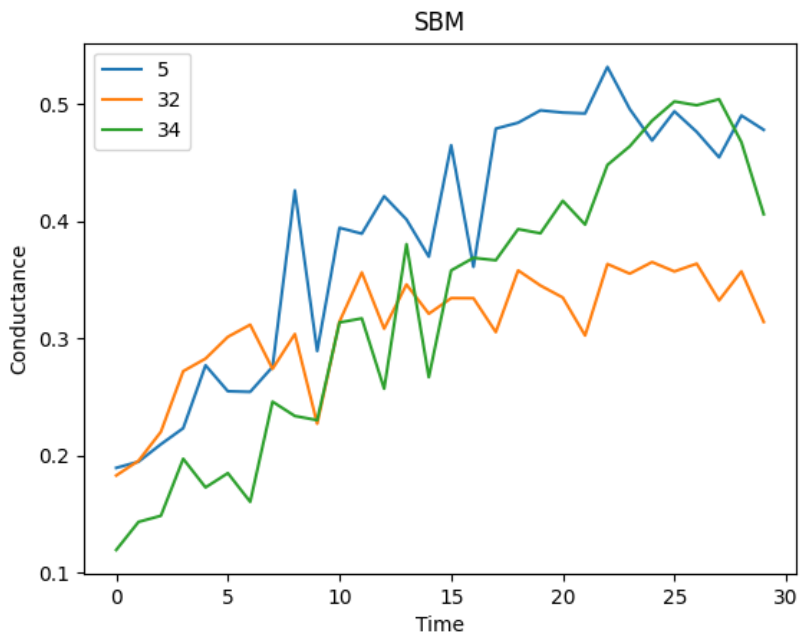

However, the above metric does not keep in mind the fact that consistent community size does not account for the fact that new nodes may be more well knit into the community than older nodes, causing older nodes to leave the community. We analyze this by taking the communities with the largest consistent size from Louvain, Label Propagation, and SBM and then analyzing the papers in them. We do this by,

- Applying the PageRank algorithm, (which is strongly correlated with number of citations, see [5]).
- Selecting the top 10 nodes based on PageRank.
- Using the arXiv API to get their paper titles, authors, and summaries.

- Analyzing the data.

Below, we show the annotated paper summaries and titles for each of the most consistent communities. More refined analysis would require a professional in the field to make comments on paper similarity, but for our purposes basic word similarity analysis shall suffice.

Label Propagation Community 12

index	arXiv ID	PageRank	Date Published	Author(s)	Title	Summary
0	9203203	0.170541533692532 8	1992-03-03T16:32:33Z	M. Dine, R. Leigh, P. Huet, A. Linde, D. Linde,	Towards the Theory of Cosmological Phase Transitions	We discuss recent progress (and controversies) in the theory of finite temperature phase transitions. This includes the structure of the effective potential at a finite temperature, the infrared problem in quantum statistics of gauge fields, the theory of formation of critical and subcritical bubbles and the theory of bubble wall propagation.
1	9203201	0.0894325320477499	1992-02-24T20:07:00Z	M. Dine, R. G. Leigh, P. Huet, A. D. Linde, D. A. Linde,	Comments on the Electroweak Phase Transition	We report on an investigation of various problems related to the theory of the electroweak phase transition. This includes a determination of the nature of the phase transition, a discussion of the possible role of higher order radiative corrections and the theory of the formation and evolution of the bubbles of the new phase. We find in particular that no dangerous linear terms appear in the effective potential. However, the strength of the first order phase transition is 2/3 times less than what follows from the one-loop approximation. This rules out baryogenesis in the minimal version of the electroweak theory.
2	9206227	0.0465000379923714 6	1992-06-17T13:44:51Z	J. R. Espinosa, M. Quirós, F. Zwirner,	On the phase transition in the scalar theory	The basic tool for the study of the electroweak phase transition is $V_{eff} (\phi,T)$, the one-loop finite-temperature effective potential, improved by all-loop resummations of the most important infrared contributions. In this paper we perform, as a first step towards a full analysis of the Standard Model case, a detailed study of the effective potential of the scalar theory. We show that subleading corrections to the self-energies lead to spurious terms, linear in the field-dependent mass $m(\phi)$, in the daisy-improved effective potential. Consistency at subleading order requires the introduction of superdaisy diagrams, which prevent the appearance of linear terms. The resulting $V_{eff}(\phi,T)$ for the scalar theory hints at a phase transition which is either second-order or very weakly first-order.
3	9206266	0.0463598126325327	1992-06-30T23:58:47Z	Stanley Myint,	Baryogenesis Constraints on the Minimal Supersymmetric Model	Requirement that the vacuum expectation values of Higgs fields immediately after the phase transition be large enough imposes constraints upon the parameters of the minimal supersymmetric model. In particular, one obtains the upper bound on the lighter CP-even Higgs mass and the soft supersymmetry breaking scale for different values of the top quark mass.
4	9208215	0.0298197171453765 2	1992-08-08T01:21:00Z	John March-Russell,	On the Possibility of Second-Order Phase Transitions in Spontaneously Broken Gauge Theories	In the ``Type-II" regime, $m_{\rm Higgs}\gap m_{\rm gauge}$, the finite-temperature phase transition in spontaneously-broken gauge theories (including the standard model) must be be studied using a renormalization group treatment. Previous studies within the $(4-\ep)$-expansion suggest a 1st-order transition in this regime. We use analogies with experimentally accessible phase transitions in liquid crystals, and theoretical investigations of superconductor phase transitions to argue that, in this range, the critical behavior of a large class of gauge-Higgs-fermion systems changes from 1st to 2nd-order as a function of Higgs mass. We identify a set of models which, within the $(2+\ep)$-expansion, possess fixed points that can describe this 2nd-order behavior. As usual, a definitive demonstration that the claimed critical behavior occurs (and a reliable estimate of $m_{\rm Higgs}$ at the tricritical point) will probably require numerical simulations. This paper uses the ``phyzzx" macro package. To obtain figure contact the author.
5	9212288	0.0249561862030996 6	1992-12-21T00:38:00Z	John Bagnasco, Michael Dine,	Some Two-Loop Corrections to the Finite Temperature Effective Potential in the Electroweak Theory	Perturbation theory at finite temperature suffers from well-known infrared problems. In the standard model, as a result, one cannot calculate the effective potential for arbitrarily small values of ϕ. the Higgs expectation value. Because the Higgs field is now known not to be extremely light, it is necessary to determine whether perturbation theory is a reliable guide to properties of the weak phase transition. In this note, we evaluate the most singular contributions to the potential at two loops as well as the leading strong interaction contributions. Above the critical temperature, the strong interaction corrections are reasonably small, while the weak corrections are about 10\%, even for rather small values of the Higgs field. At the critical temperature, the weak corrections have a more substantial effect, rendering the transition significantly more first order, but not significantly changing the upper bound on the Higgs mass required for baryogenesis.
6	9212224	0.02273522003302	1992-12-05T00:57:10Z	P. Huet, K. Kajantie, R. G. Leigh, B. -H. Liu, L. McLerran,	Hydrodynamic Stability Analysis of Burning Bubbles in Electroweak Theory and in QCD	Assuming that the electroweak and QCD phase transitions are first order, upon supercooling, bubbles of the new phase appear. These bubbles grow to macroscopic sizes compared to the natural scales associated with the Compton wavelengths of particle excitations. They propagate by burning the old phase into the new phase at the surface of the bubble. We study the hydrodynamic stability of the burning and find that for the velocities of interest for cosmology in the electroweak phase transition, the shape of the bubble wall is stable under hydrodynamic perturbations. Bubbles formed in the cosmological QCD phase transition are found to be a borderline case between stability and instability.
7	9303317	0.0211286147535402 97	1993-03-30T19:41:55Z	J. R. Espinosa, M. Quiros, F. Zwirner,	On the electroweak phase transition in the Minimal Supersymmetric Standard Model	We study the finite-temperature effective potential of the Minimal Supersymmetric Standard Model, in the limit of only one light Higgs boson. Because of the large top Yukawa coupling, there can be significant differences with respect to the Standard Model case. for given values of the Higgs and top masses, little supersymmetry breaking in the stop sector can make the phase transition more strongly first-order. After including the full structure of the stop mass matrix, the most important experimental constraints and the leading plasma effects, we find that the present limits on Higgs and squark masses are still compatible with the scenario of electroweak baryogenesis, in a small region of parameter space corresponding to $m_h \simlt 70 \gev$ and $\msbs \simlt 105 \gev$.
8	9306238	0.0180330726544449 9	1993-06-07T15:09:00Z	D. Boyanovsky, C. A. de Carvalho,	Real Time Analysis of Thermal Activation via Sphaleron Transitions	We study the process of thermal activation mediated by sphaleron transitions by analyzing the real-time dynamics of the decay out of equilibrium in a $1+1$ dimensional field theory with a metastable state. The situation considered is that of a rapid supercooling in which the system is trapped in a metastable state at a temperature larger than the mass of the quanta, but smaller than the energy to create a critical droplet. The initial density matrix is evolved in time and the nucleation rate (probability current at the saddle point) is computed. The nucleation rate is (\it time dependent), vanishing at early times, reaching a maximum at a time $t \approx 1/m$ with m the mass of quanta in the metastable state, and decreasing at long times as a consequence of unitarity. An estimate for the average number of particles of ``true vacuum" produced as a function of time during the nucleation process is obtained.
9	9308364	0.0163069324555045	1993-08-31T03:58:16Z	Mark Alford, John March-Russell,	Radiatively-Induced First-Order Phase Transitions: The Necessity of the Renormalization Group	We advocate a (Wilson) renormalization-group (RG) treatment of finite-temperature first-order phase transitions, in particular those driven by radiative corrections such as occur in the standard model, and other spontaneously-broken gauge theories. We introduce the scale-dependent coarse-grained free energy $S_\Lat[\phi]$ which we explicitly calculate, using the Wilson RG and a $(4-\ep)$-expansion, for a scalar toy model that shares many features of the gauged case. As argued by Langer and others, the dynamics of the phase transition are described by $S_\Lat[\phi]$ with $\Lat$ of order the bubble wall thickness, and (\it not) by the usual (RG-improved) finite-temperature effective action which is reproduced by $S_\Lat[\phi]$ for $\Lat\to 0$. We argue that for weakly first-order transitions (such as that in the standard model) the $(4-\ep)$-expansion is necessary to control an inevitable growth of the effective scale-dependent coupling towards the strong-coupling regime, and that diagrammatic resummation techniques are unlikely to be appropriate.

Label Propagation Community 23

index	arXiv ID	PageRank	Date Published	Author(s)	Title	Summary
0	9307226	0.165258061360191 94	1993-07-06T17:53:36Z	G. F. Giudice, E. Roulet,	Conditions on supersymmetry soft-breaking terms from GUTs	We study the effect of integrating out the heavy fields in a supersymmetric GUT which does not contain small mass parameters in the limit of exact supersymmetry. The trilinear (A) and bilinear (B) coefficients of the supersymmetry soft-breaking terms of the low-energy effective theory are related in a simple and model-independent way to those of the underlying theory. (|From these relations, we obtain the bound $\|B\|\ge 2$, which, together with the requirements of stability of the potential and electroweak symmetry breaking, imposes severe constraints on the space of allowed supersymmetric parameters. In models based on supergravity with a flat Kˈahler metric, we obtain $B=2$, instead of the relation $B=A-1$ usually used in phenomenological applications. The low-energy theory contains also a supersymmetric mass term μ for the two Higgs doublets, which is of the order of the supersymmetry-breaking scale.
1	9403306	0.123840708293591 41	1994-03-17T21:01:05Z	Paul Langacker, Nir Polonsky,	Implications of Yukawa unification for the Higgs sector in supersymmetric grand-unified models	The SU(5) unification-scale relation h_b=h_tau between the b and tau Yukawa couplings severely constrains tan beta and m_t (even more so if h_t=h_b= h_tau holds) in supersymmetric models. We examine the implications of these constraints for the Higgs sector assuming universal soft breaking terms, and emphasize that both of these relations impose unique characteristics in terms of symmetries and of the spectrum. We further study the tan beta near 1 scenario, which is suggested by h_b=h_tau, and, in particular, the loop- induced mass of the light Higgs boson. We compare the effective potential and renormalization group methods and stress the two-loop ambiguities in the calculation of the mass. These and a large enhancement to the loop correction due to t-scalar left-right mixing considerably weaken the upper bound. Nevertheless, we find that for this scenario the Higgs boson is probably lighter than 110 GeV, and typically lighter than 100 GeV. Thus, it is in the mass range that may be relevant for LEPII. Our numerical results are presented in a self-contained manner in section V. In separate appendices we discuss the global symmetries of the Higgs potential, the issue of false (color-breaking) vacua, two-loop calculations, and the effect of an additional Higgs singlet. We show that the approximate constraints that are often used to eliminate color-breaking vacua are not always relevant.
2	9402254	0.0905952621937380 1	1994-02-09T05:18:00Z	Yoshiharu Kawamura, Hiloshi Murayama, Masahiro Yamaguchi,	Probing Symmetry-Breaking Pattern Using Sfermion Masses	We study the mass spectrum of superparticles within supersymmetric grand unified models. For gaugino masses, it is pointed out that the GUT-relation in the $SU(5)$ model is applicable to a more general case where a grand-unified gauge group breaks down to the standard model gauge group by several steps. We also show that the mass spectrum of squarks and sleptons carries the information on the breaking pattern of the gauge symmetry. It is demonstrated in some $SO(10)$ models how the scalar mass spectrum distinguishes various $SO(10)$ breaking patterns from each other.
3	9405252	0.0691312680193451 3	1994-05-09T12:52:55Z	Ralf Hempfling,	On the fine-tuning problem in minimal SO(10) SUSY-GUT	In grand unified theories (GUT) based on SO(10) all fermions of one generation are embedded in a single representation. As a result, the top quark, the bottom quark, and the τ lepton have a universal Yukawa coupling at the GUT scale. This implies a very large ratio of Higgs vacuum expectation values, $\tan\ \simeq m_t/m_b$. We analyze the naturalness of such a scenario quantitatively including all the relevant radiative corrections and find that in minimal unified supergravity models with universal soft supersymmetry breaking parameters at the GUT scale, the necessary amount of fine-tuning needed is excessive. GUT threshold correction to the universal Higgs mass parameter can significantly reduce the fine-tuning required for such large values of $\tan\beta$. We also point out that the top quark mass can play a crucial role in explaining the hierarchy between the SUSY breaking scale and the electro-weak scale and, hence, the naturalness of large values of $\tan\beta$.
4	9411276	0.0674652734434573 7	1994-11-11T23:24:23Z	H. -C. Cheng, L. J. Hall,	Squark and Slepton Mass Relations in Grand Unified Theories	In the minimal supersymmetric standard model, assuming universal scalar masses at large energies, there are four intragenerational relations between the masses of the squarks and sleptons for each light generation. In this paper we study the scalar mass relations which follow only from the assumption that at large energies there is a grand unified theory which leads to a significant prediction of the weak mixing angle. Two new intragenerational mass relations for each of the light generations are derived. In addition, a third mass relation is found which relates the Higgs masses, the masses of the third generation scalars , and the masses of the scalars of the lighter generations. Verification of a fourth mass relation, involvingonly the charged slepton masses, provides a signal for SO(10) unification.
5	9410231	0.0638702149595733 3	1994-10-06T11:37:45Z	Nir Polonsky, Alex Pomarol,	Non-Universal GUT Corrections to the Soft Terms and their Implications in Supergravity Models	Potentially large non-universal corrections to the soft supersymmetry breaking parameters arise from their evolution between the Planck and the grand-unification scales. We detail typical patterns of non-universality in GUT models, as well as elaborate on their propagation to the weak scale and on their low-energy implications. Possible corrections to the different scalar quark and lepton masses and the Higgs and the gaugino-Higgsino sector parameters are described in detail, and new allowed regions of the parameter space are pointed out. In particular, the patterns studied often lead to heavier Higgsinos and t-scalar. One-loop GUT threshold corrections to the soft parameters are also discussed and shown to be important.
6	9407404	0.0638702149595733 3	1994-07-29T17:18:53Z	M. Olechowski, S. Pokorski,	Electroweak Symmetry Breaking with Non-Universal Scalar Soft Terms and Large $\tan\beta$ Solutions	We discuss radiative electroweak symmetry breaking with non-universal scalar masses at the GUT scale. Large $\tan\beta$ solutions are investigated in detail and it is shown that qualitatively new (as compared to the universal case) solutions exist, with much less correlation between soft terms. We identify two classes of non-universalities which give solutions with $A_o\simeq B_o\simeq M_{1/2}\simeq O(M_Z)$, $\mu \simeq O(0.5 m_o)$, $m_o>>M_Z$ and $A_o\simeq B_o\simeq M_{1/2} \simeq\mu\simeq O(M_Z)$, $m_o\ge M_Z$, respectively. In each case, after imposing gauge and Yukawa coupling unification, we discuss the predictions for m_t, m_b and the spectrum of supersymmetric particles. One striking consequence is the possibility of light charginos and neutralinos which in the second option can be higgsino-like. Cosmological constraint on the relic abundance of the lightest neutralino is also included.
7	9407251	0.0638702149595733 3	1994-07-07T15:29:40Z	D. Matalliotakis, H. P. Nilles,	Implications of non-universality of soft terms in supersymmetric grand unified theories	Most discussions of supersymmetric grand unified theories assume universality of the soft supersymmetry breaking terms at the grand scale. We point out that the behaviour of these theories might change significantly in the presence of non--universal soft terms. Particularly in SO(10)--like models with a large value of tanβ we observe a decisive change of predictions, allowing the presence of relatively light gauginos as well as small supersymmetric corrections to the b--quark mass. Some results remain rather stable, including the μ--$M_{1/2}$ correlation. Models with small tanβ seem to be less affected by non--universality which mainly leads to the new possibility of small m_{0} (i.e. the squark and slepton soft mass parameter), excluded in the universal case.
8	9304218	0.0599934757891053	1993-04-05T18:35:24Z	John S. Hagelin, S. Kelley, Toshiaki Tanaka,	Exact Supersymmetric Amplitude for \kbbV and \bbbV Mixing	We present the most general supersymmetric amplitude for \kbbV and \bbbV mixing resulting from gluino box diagrams. We use this amplitude to place general constraints on the magnitude of flavor-changing squark mass mixings, and compare these constraints to theoretical predictions both in and beyond the Minimal Supersymmetric Standard Model.
9	9503445	0.0464210612043701 45	1995-03-27T18:14:47Z	Chris Kolda, Stephen P. Martin,	Low-energy supersymmetry with D-term contributions to scalar masses	We investigate how the predictions of the Minimal Supersymmetric Standard Model are modified by D-term contributions to soft scalar masses, which arise whenever the rank of the gauge group at very high energies is greater than four. We give a parameterization of the most general such contributions that can occur when the unbroken gauge symmetry is an arbitrary subgroup of E_6, and show how the D-term contributions leave their imprint on physics at ordinary energies. We impose experimental constraints on the resulting parameter space and discuss some features of the resulting supersymmetric spectrum which differ from the predictions obtained with universal boundary conditions on scalar masses near the Planck scale. These include relations between squark and slepton masses; the behavior of $\sin^2 (\beta-\alpha)$ (which determines the production cross-section for the lightest Higgs scalar boson at an e+e- collider) and the mass of the pseudoscalar Higgs bosons; R_b [the ratio $\Gamma(Z -> b\overline b)/\Gamma(Z -> hadrons)$; and mass differences between charginos and neutralinos.

Label Propagation Community 42

index	arXiv ID	PageRank	Date Published	Author(s)	Title	Summary
0	9302280	0.11150528460785714	1993-02-19T19:08:00Z	Z. Bern, L. Dixon, D. A. Kosower,	One-Loop Corrections to Five-Gluon Amplitudes	We present the one-loop helicity amplitudes with five external gluons. The computation employs string-based methods, new techniques for performing tensor integrals, and improvements in the spinor helicity method.
1	9205205	0.10159790688509066	1992-05-05T18:25:00Z	Matthew J. Strassler,	Field Theory Without Feynman Diagrams: One-Loop Effective Actions	In this paper the connection between standard perturbation theory techniques and the new Bern-Kosower calculational rules for gauge theory is clarified. For one-loop effective actions of scalars, Dirac spinors, and vector bosons in a background gauge field, Bern-Kosower-type rules are derived without the use of either string theory or Feynman diagrams. The effective action is written as a one-dimensional path integral, which can be calculated to any order in the gauge coupling; evaluation leads to Feynman parameter integrals directly, bypassing the usual algebra required from Feynman diagrams, and leading to compact and organized expressions. This formalism is valid off-shell, is explicitly gauge invariant, and can be extended to a number of other field theories.
2	9207266	0.05082013720836507	1992-07-28T12:29:00Z	C. S. Lam,	Navigating Around the Algebraic Jungle of QCD: Efficient Evaluation of Loop Helicity Amplitudes	A method is developed whereby spinor helicity techniques can be used to simplify the calculation of loop amplitudes. This is achieved by using the Feynman-parameter representation where the offending off-shell loop momenta do not appear. Background Feynman gauge also helps to simplify the calculations. This method is applicable to any Feynman diagram with any number of loops as long as the external masses can be ignored, and it is at least as efficient as the string technique in the special circumstances when the latter can be used. In order to minimize the very considerable algebra encountered in non-abelian gauge theories, graphical methods are developed for most of the calculations. This enables the large number of terms encountered to be organized visually in the Feynman diagram without the necessity of having to write down any of them algebraically. A one-loop four-gluon amplitude in a particular helicity configuration is computed explicitly to illustrate the method.
3	9212308	0.04589863700818097	1992-12-24T22:32:49Z	Z. Bern, L. Dixon, D. A. Kosower,	Dimensionally Regulated One-Loop Integrals	We describe methods for evaluating one-loop integrals in $4-2\e$ dimensions. We give a recursion relation that expresses the scalar n-point integral as a cyclicly symmetric combination of $(n-1)$-point integrals. The computation of such integrals thus reduces to the calculation of box diagrams ($n=4$). The tensor integrals required in gauge theory may be obtained by differentiating the scalar integral with respect to certain combinations of the kinematic variables. Such relations also lead to differential equations for scalar integrals. For box integrals with massless internal lines these differential equations are easy to solve.
4	9210213	0.04033677317199301	1992-10-05T18:14:29Z	G. Mahlon, T. M. Yan,	Multiphoton Production at High Energies in the Standard Model I	We examine multiphoton production in the electroweak sector of the Standard Model in the high energy limit using the equivalence theorem in combination with spinor helicity techniques. We obtain recursion relations for currents consisting of a charged scalar, spinor, or vector line that radiates n photons. Closed form solutions to these recursion relations for arbitrary n are presented for the cases of like-helicity and one unlike-helicity photon production. We apply the currents singly and in pairs to obtain amplitudes for processes involving the production of n photons with up to two unlike helicities from a pair of charged particles. The replacement of one or more photons by transversely polarized $SU(2)$-bosons is also discussed.
5	9312276	0.03654822227863767	1993-12-14T15:11:49Z	Gregory Mahlon,	Multigluon Helicity Amplitudes Involving a Quark Loop	We apply the solution to the recursion relation for the double-off-shell quark current to the problem of computing one-loop amplitudes with an arbitrary number of gluons. We are able to compute amplitudes for photon-gluon scattering, electron-positron annihilation to gluons, and gluon-gluon scattering via a quark loop in the case of like-helicity gluons. In addition, we present the result for the one-loop gluon-gluon scattering amplitude when one of the gluons has opposite helicity from the others.
6	9305239	0.03584492792062275	1993-05-11T13:25:16Z	Zoltan Kunszt, Adrian Signer, Zoltán Trócsányi,	One-loop helicity amplitudes for all 2 -> 2 processes in QCD and N=1 supersymmetric Yang-Mills theory	One-loop corrections to the helicity amplitudes of all 2 -> 2 subprocesses are calculated in QCD and in N=1 supersymmetric Yang-Mills theory using two versions of dimensional regularization: the ^t-Hooft-Veltman scheme and dimensional reduction. Studying the structure of the soft and collinear singularities, we found universal transition rules for the squared matrix element which can be used to translate the results obtained in these schemes to the results valid in the conventional dimensional regularization scheme. With explicit calculation it is demonstrated that the one-loop helicity amplitudes of the 2 -> 2 subprocesses calculated using dimensional reduction in the N=1 supersymmetric $SU(N)$ gauge theory respect the supersymmetry Ward identities. Our transition rules can also be used to calculate the next-to-leading order Altarelli-Parisi kernels in the dimensional reduction scheme when they satisfy supersymmetry Ward identities as well.
7	9311213	0.03379138271602818	1993-11-02T22:28:39Z	Gregory Mahlon,	One-Loop Multiphoton Helicity Amplitudes	We use the solutions to the recursion relations for double-off-shell fermion currents to compute helicity amplitudes for n-photon scattering and electron-positron annihilation to photons in the massless limit of QED. The form of these solutions is simple enough to allow {\t all}\ of the integrations to be performed explicitly. For n-photon scattering, we find that unless $n=4$, the amplitudes for the helicity configurations (+++...+) and (-++...+) vanish to one-loop order.
8	9210214	0.03355739564835179	1992-10-05T18:14:58Z	G. Mahlon,	Multiphoton Production at High Energies in the Standard Model II	We examine multiphoton production in the electroweak sector of the Standard Model in the high energy limit using the equivalence theorem in combination with spinor helicity techniques. We utilize currents consisting of a charged scalar, spinor, or vector line that radiates n photons. Only one end of the charged line is off shell in these currents, which are known for the cases of like-helicity and one unlike-helicity photons. We obtain a wide variety of helicity amplitudes for processes involving two pairs of charged particles by considering combinations of four currents. We examine the situation with respect to currents which have both ends of the charged line off-shell, and present solutions for the case of like-helicity photons. These new currents may be combined with two of the original currents to produce additional amplitudes involving Higgs, longitudinal Z or neutrino pairs.
9	9210212	0.03355739564835179	1992-10-05T18:13:55Z	G. Mahlon, T. M. Yan, C. Dunn,	Generalized Gluon Currents and Applications in QCD	We consider the process containing two quark lines and an arbitrary number of gluons in a spinor helicity framework. A current with two off-shell gluons appears in the amplitude. We first study this modified gluon current using recursion relations. The recursion relation for the modified gluon current is solved for the case of like-helicity gluons. We apply the modified gluon current to compute the amplitude for $q \bar q \rightarrow q \bar q gg \cdots g$ in the like-helicity gluon case.

Label Propagation Community 54

index	arXiv ID	PageRank	Date Published	Author(s)	Title	Summary
0	9209203	0.12739555287798919	1992-09-01T20:12:14Z	Lowell S. Brown,	Summing tree graphs at threshold	The solution of the classical field equation generates the sum of all tree graphs. We show that the classical equation reduces to an easily solved ordinary differential equation for certain multiparticle threshold amplitudes and compute these amplitudes.
1	9209240	0.08583090452152847	1992-09-15T19:45:07Z	M. B. Voloshin,	Summing One-Loop Graphs at Multi-Particle Threshold	It is shown that the technique recently suggested by Lowell Brown for summing the tree graphs at threshold can be extended to calculate the loop effects. Explicit result is derived for the sum of one-loop graphs for the amplitude of threshold production of n on-mass-shell particles by one virtual in the unbroken $\lambda \phi^4$ theory. It is also found that the tree-level amplitude of production of n particles by two incoming on-mass-shell particles vanishes at the threshold for $n > 4$.
2	9212280	0.05242528665118087	1992-12-18T09:46:27Z	E. N. Argyres, C. G. Papadopoulos, R. Kleiss,	On amplitude zeros at threshold	The occurrence of zeros of 2 to n amplitudes at threshold in scalar theories is studied. We find a differential equation for the scalar potential, which incorporates all known cases where the 2 to n amplitudes at threshold vanish for all sufficiently large n, in all space-time dimensions, $d\ge 1$. This equation is related to the reflectionless potentials of Quantum Mechanics and to integrable theories in 1+1 dimensions. As an application, we find that the sine-Gordon potential and its hyperbolic version, the sinh-Gordon potential, also have amplitude zeros at threshold, $\{\cal A}(2\to n)=0$, for $n\ge 4$ and $d\ge 2$, independently of the mass and the coupling constant.
3	9210244	0.04111664960339377	1992-10-19T15:54:38Z	M. B. Voloshin,	Zeros of Tree-Level Amplitudes at Multi-Boson Thresholds	Propagation of particles with emission of arbitrary number of identical bosons all being at rest is considered. It is shown that in certain models the tree-level amplitudes for production of n scalar bosons by two incoming particles are all equal to zero at the threshold starting from some small number n. In particular this nullification occurs for production of massive scalars by two Goldstone bosons in the linear sigma model for $n > 1$ and also for production of Higgs bosons in the Standard Model by gauge bosons and/or by fermions, provided that the ratio of their masses to that of the Higgs boson take special discrete values.
4	9303321	0.03569229669917566	1993-03-31T19:48:36Z	E. N. Argyres, Ronald H. P. Kleiss, Costas G. Papadopoulos,	Multiscalar amplitudes to all orders in perturbation theory	A method for calculating loop amplitudes at the multiboson threshold is presented, based on Feynman-diagram techniques. We explicitly calculate the one-loop amplitudes in both ϕ^4-symmetric and broken symmetry cases, using dimensional regularization. We argue that, to all orders in the perturbation expansion, the unitarity-violating behaviour of the tree-order amplitudes persists.
5	9305219	0.03192638505225127	1993-05-06T21:44:40Z	A. S. Gorsky, M. B. Voloshin,	Non-Perturbative Production of Multi-Boson States and Quantum Bubbles	The amplitude of production of n on-mass-shell scalar bosons by a highly virtual field ϕ is considered in a $\lambda \phi^4$ theory with weak coupling λ and spontaneously broken symmetry. The amplitude of this process is known to have an $n!$ growth when the produced bosons are exactly at rest. Here it is shown that for $n \gg 1/\lambda$ the process goes through `quantum bubbles', i.e. quantized droplets of a different vacuum phase, which are non-perturbative resonant states of the field ϕ. The bubbles provide a form factor for the production amplitude, which rapidly decreases above the threshold. As a result the probability of the process may be heavily suppressed and may decrease with energy E as $\exp (-const \cdot E^a)$, where the power a depends on the number of space dimensions. Also discussed are the quantized states of bubbles and the amplitudes of their formation and decay.
6	9209287	0.03150448448124143	1992-09-28T21:37:52Z	B. H. Smith,	Summing one-loop graphs in a theory with broken symmetry	The method suggested by Lowell Brown for calculating multi-particle threshold amplitudes is extended to the one-loop level in scalar theories with broken reflection symmetry. A result for the threshold amplitude for multiparticle production is derived. It is also shown that the tree-level amplitude for 2 on-mass-shell particles producing n particles vanishes at the kinematical threshold for $n>2$.
7	9303322	0.03094246627839593	1993-03-31T19:52:30Z	E. N. Argyres, R. Kleiss, C. G. Papadopoulos,	Nullification of multi-Higgs threshold amplitudes in the Standard Model	We show that nullification of all tree-order threshold amplitudes involving Higgs particles in the Standard Model occurs, provided that certain equations relating the masses of all existing elementary particles to the mass of the Higgs scalar are satisfied. The possible role of these relations in restoring the high-multiplicity unitarity and their phenomenological relevance are briefly discussed.
8	9301255	0.02756500946553357	1993-01-21T15:42:40Z	Brian Hendee Smith,	Calculation of processes involving many particles at the kinematical threshold	A diagrammatic technique is derived for calculating processes involving the production of large numbers of particles. As an example, the amplitude of three particles scattering into n particles at the kinematical threshold in $\lambda\phi^4$ theory is calculated. From the $3 \to n$ amplitude, it is seen that the one-loop amplitude for $2 \to n$ processes is suppressed by a factor of $1/n$.
9	9307213	0.02660901747026162	1993-07-02T14:42:26Z	M. V. Libanov, V. A. Rubakov, S. V. Troitsky,	Tree amplitudes at multiparticle threshold in a model with softly broken $O(2)$ symmetry	Tree amplitudes of the production of two kinds of scalar particles at threshold from one virtual particle are calculated in a model of two scalar fields with $O(2)$ symmetric quartic interaction and unequal masses. These amplitudes exhibit interesting factorial and exponential behaviour at large multiplicities. As a by-product we observe that the kinematically allowed decay of one real particle into n real particles of another kind, all at rest, has zero tree amplitude in this model for $n>2$.

Label Propagation Community 59

index	arXiv ID	PageRank	Date Published	Author(s)	Title	Summary
0	9306289	0.15145218548098943	1993-06-18T16:50:00Z	F. E. Close, R. G. Roberts,	Consistent Analysis of the Spin Content of the Nucleon	The recent measurements of lepton nucleon scattering with polarised neutron and deuteron targets are analysed together with the previous polarised proton data in a mutually consistent way. The detailed x-dependence of the polarisation asymmetry in the valence region is shown to be in agreement with historical predictions based on quark models. The Bjorken sum rule is shown to be confirmed at the 1σ level and estimates of the spin content of the nucleon Δq are extracted. While the average value of Δq from the three experiments comes out to be 0.41 ± 0.05 (to be compared with the naive quark model theoretical expectation of 0.58) this experimental average value is more than one standard deviation from the value obtained from any individual experiment.This inconsistency can be overcome by allowing arbitrary higher twist contributions but the resulting precision is poor, $\Delta q = 0.38\pm 0.48$.
1	9305306	0.09718671994363874	1993-05-24T14:18:31Z	John Ellis, Marek Karliner,	Analysis of Data on Polarized Lepton-Nucleon Scattering	We re-analyze data on deep inelastic polarized lepton-nucleon scattering, with particular attention to testing the Bjorken sum rule and estimating the quark contributions to the nucleon spin. Since only structure function data at fixed Q^2 can be used to test sum rules, we use E142 asymmetry measurements and unpolarized structure function data to extract g_1^n at fixed Q^2 = 2 GeV^2. When higher-twist effects, which are important at low Q^2, are included, both the E142 and SMC data are compatible with the Bjorken sum rule within one standard deviation. Assuming validity of the Bjorken sum rule, we estimate the quark contributions to the nucleon spin, finding that their total net contribution is small, with the strange quark contribution non-zero and negative. The quark spin content of the nucleon spin is in agreement with Skyrme model.
2	9404270	0.09389145631566512	1994-04-15T08:56:12Z	the SMC,	Measurement of the Spin-Dependent Structure Function $g_1(x)$ of the Proton	We have measured the spin-dependent structure function g_1^p of the proton in deep inelastic scattering of polarized muons off polarized protons, in the kinematic range $0.003<x<0.75$ and $1\,\mbox{GeV}^2<Q^2<60\,\mbox{GeV}^2$. Its first moment, $\int_0^1 g_1^p(x) dx $, is found to be $0.136 \pm 0.011\,(\mbox{stat.})\pm 0.011\,(\mbox{syst.})$ at $Q^2=10\,\mbox{GeV}^2$. This value is smaller than the prediction of the Ellis--Jaffe sum rule by two standard deviations, and is consistent with previous measurements. A combined analysis of all available proton, deuteron and neutron data confirms the Bjorken sum rule to within 10% of the theoretical value.
3	9311255	0.06219572040835065	1993-11-10T08:41:00Z	G. Altarelli, P. Nason, G. Ridolfi,	On the Q^2 Dependence of Measured Polarized Structure Funtions	We analyse the available data on the polarized asymmetries A_1 for proton, neutron and deuteron targets. We use a homogeneous and updated set of unpolarized structure functions to derive g_1 from A_1, and we accurately correct for the scaling violations in order to obtain $g_1(x,Q^2)$ with the same Q^2 for all x values. The contribution to the Q^2 evolution of a possible large gluon polarized density is also considered. The implications for the Ellis-Jaffe and for the Bjorken sum rules are discussed.
4	9403383	0.01906853121052201	1994-03-29T08:09:31Z	S. A. Larin,	The next-to-leading QCD approximation to the Ellis-Jaffe sum rule	The \alpha_s^2 correction to the Ellis-Jaffe sum rule for the structure function g_1 of polarized deep inelastic lepton-nucleon scattering is calculated.
5	9310272	0.01884683290190507 2	1993-10-12T16:06:00Z	John Ellis, Marek Karliner,	Spin Structure Functions	We review the theory and phenomenology of deep inelastic polarized lepton-nucleon scattering in the light of recent data with a deuteron target from the SMC at CERN and a Helium 3 target from the E142 experiment at SLAC. After including higher-order perturbative QCD corrections, mass corrections and updated estimates of higher-twist effects, we find good agreement with the basic Bjorken sum rule, and extract a consistent set of values for the quark contributions to the proton spin: $$\Delta\Sigma \equiv \Delta u + \Delta d + \Delta s = 0.27 \pm 0.11 $$ $$\Delta u = 0.82 \pm 0.04, \Delta d = -0.44 \pm 0.04,\Delta s = -0.11 \pm 0.04 $$ which are consistent with chiral soliton models and indications from lattice estimates. We also mention the prospects for future experiments on the spin structure of the nucleon.
6	9309336	0.01876026150243034	1993-09-30T08:04:44Z	T. Morii, S. Tanaka, T. Yamanishi,	Effects of the large gluon polarization on $xg_1^d(x)$ and J/ψ productions at polarized ep and pp collisions	The recent SMC data of $xg_1^d(x)$ are reproduced with the large polarized gluons. To study further the polarized gluon distribution in a proton, we calculate the spin--dependent differential cross section for J/ψ leptoproductions and the two--spin asymmetry for J/ψ hadroproductions. Its experimental implication is discussed.
7	9407287	0.01735327615613733 3	1994-07-13T13:39:00Z	John Ellis, Marek Karliner,	Determination of a_s and the Nucleon Spin Decomposition Using Recent Polarized Structure Function Data	New data on polarized $\mu-p$ and $e-p$ scattering permit a first determination of α_s using the Bjorken sum rule, as well as higher precision in determining the nucleon spin decomposition. Using perturbative QCD calculations to $O(\alpha_s^3)$ for the non-singlet combination of structure functions, we find $\alpha_s(2.5 GeV^2) = 0.375^{+0.062}_{-0.081}$, corresponding to $\alpha_s(M_Z^2) =0.122^{+0.005}_{-0.009}$, and using calculations to $O(\alpha_s^3)$ for the singlet combination we find $\Delta u = 0.83 \pm 0.03$, $\Delta d= -0.43 \pm 0.03$, $\Delta s =-0.10 \pm 0.03$, $\Delta \Sigma \equiv \Delta u + \Delta d + \Ds = 0.31 \pm 0.07$, at a renormalization scale $Q^2=10 GeV^2$. Perturbative QCD corrections play an essential role in reconciling the interpretations of data taken using different targets. We discuss higher-twist uncertainties in these determinations. The Δq determinations are used to update predictions for the couplings of massive Cold Dark Matter particles and axions to nucleons.
8	9212257	0.01642122297911392 8	1992-12-14T14:50:35Z	Véronique Bernard, Norbert Kaiser, Ulf-G. Meißner,	Small Momentum Evolution of the Extended Drell--Hearn--Gerasimov Sum Rule	We investigate the momentum dependence of the extended Drell-Hearn-Gerasimov sum rule. An economical formalism is developed which allows to express the extended DHG sum rule in terms of a single virtual Compton amplitude in forward direction. Rigorous results for the small momentum evolution are derived from chiral perturbation theory within the one-loop approximation. Furthermore, we evaluate some higher order contributions arising from $\Delta(1232)$ intermediate states and relativistic corrections. (2 figures available upon request).
9	9310306	0.01573923538759409	1993-10-18T15:19:20Z	S. D. Bass, A. W. Thomas,	The Spin Structure of the Nucleon	We provide an introduction to the ideas of spin-dependent deep-inelastic scattering. Recent experimental results are summarised and possible explanations related to the axial anomaly presented. Further experiments that could greatly clarify the situation are also described.

Louvain Community 0

index	arXiv ID	PageRank	Date Published	Author(s)	Title	Summary
0	9212203	0.011085825811781526	1992-12-01T22:24:05Z	M. Ciuchini, E. Franco, G. Martinelli, L. Reina,	$c^{\prime}/c$ at the next-to-leading order in QCD and QED	We present a new calculation of the CP violation parameter $\epsilon^{\prime}/ \epsilon$. The results reported in this paper have been obtained by using the $\Delta S=1$ effective Hamiltonian computed at the next-to-leading order, including QCD and QED penguins. The matrix elements of the relevant operators have been taken from lattice QCD, at a scale $\mu=2$ GeV. At this relatively large scale, the perturbative matching between the relevant operators and the corresponding coefficients is quite reliable. The effect of the next-to-leading corrections is to lower the prediction obtained at the leading order, thus favouring the experimental result of E731. We analyze different contributions to the final result and compare the leading and next-to-leading cases.
1	9303284	0.004374476590532856	1993-03-19T08:53:27Z	Andrzej J. Buras, Matthias Jamin, Markus E. Lautenbacher,	The Anatomy of ε'/ε Beyond Leading Logarithms with Improved Hadronic Matrix Elements	We use the recently calculated two--loop anomalous dimensions of current-current operators, QCD and electroweak penguin operators to construct the effective Hamiltonian for $\Delta S=1$ transitions beyond the leading logarithmic approximation. We solve the renormalization group equations and give the numerical values of Wilson coeff. functions. We propose a new semi-phenomenological approach to hadronic matrix elements which incorporates the data for CP-conserving $K \rightarrow \pi\pi$ amplitudes and allows to determine the matrix elements of all $(V-A)\otimes (V-A)$ operators in any renormalization scheme and do a renormalization group analysis of all hadronic matrix elements $\langle Q_i(\mu) \rangle$. We compare critically our treatment of these matrix elements with those given in the literature. We find in the NDR scheme $\epe = (6.7 \pm 2.6)\times 10^{-4}$ in agreement with the experimental findings of E731. We point out however that the increase of $\langle Q_6 \rangle$ by only a factor of two gives $\epe = (20.0 \pm 6.5)\times 10^{-4}$ in agreement with the result of NA31. The dependence of $\epe$ on $\Lambda_{\bar{MS}}$, m_t and $\langle Q_{6,8} \rangle$ is presented.
2	9403339	0.003586030121082364 7	1994-03-22T15:50:45Z	Chang-Hwan Lee, G. E. Brown, Mannque Rho,	Kaon Condensation in ``Nuclear Star" Matter	The critical density for kaon condensation in ``nuclear star" matter is computed up to two-loop order (\it in medium) (corresponding to next-to-next-to-leading order in chiral perturbation theory in free space) with a heavy-baryon effective chiral Lagrangian whose parameters are determined from KN scattering and kaonic atom data. To the order considered, the kaon self-energy has highly non-linear density dependence in dense matter. We find that the four-Fermi interaction terms in the chiral Lagrangian play an important role in triggering condensation, predicting for ``natural" values of the four-Fermi interactions a rather low critical density, $\rho_c < 4 \rho_0$.
3	9304257	0.003064899836085560 4	1993-04-15T16:31:44Z	M. Ciuchini, E. Franco, G. Martinelli, L. Reina,	The $\Delta S=1$ Effective Hamiltonian Including Next-to-Leading Order QCD and QED Corrections	In this paper we present a calculation of the $\Delta S=1$ effective weak Hamiltonian including next-to-leading order QCD and QED corrections. At a scale μ of the order of few GeV, the Wilson coefficients of the operators are given in terms of the renormalization group evolution matrix and of the coefficients computed at a large scale $\simeq M_W$. The expression of the evolution matrix is derived from the two-loop anomalous dimension matrix which governs the mixing of the relevant current-current and penguin operators, renormalized in some given regularization scheme. We have computed the anomalous dimension matrix up to and including order $\alphas^2$ and $\alphae \alphas$ in two different renormalization schemes, NDR and HV, with consistent results. We give many details on the calculation of the anomalous dimension matrix at two loops, on the determination of the Wilson coefficients at the scale M_W and of their evolution from M_W to μ. We also discuss the dependence of the Wilson coefficients/operators on the regularization scheme.
4	9406263	0.003002100530586003 7	1994-06-09T13:48:11Z	C. R. Allton, M. Ciuchini, M. Crisafulli, E. Franco, V. Lubicz, G. Martinelli,	Quark Masses from Lattice QCD at the Next-to-Leading Order	Using the results of several quenched lattice simulations, we predict the value of the strange and charm quark masses in the continuum at the next-to-leading order, $m^{\overline{MS}}_s(\mu=2\,\, \mathrm{GeV})= (127 \pm 18)\,\, \mathrm{MeV}$ and $m^{\overline{MS}}_{ch}(\mu=2 \,\,\mathrm{GeV})=(1.47 \pm 0.28)\,\, \mathrm{GeV}$. The errors quoted above have been estimated by taking into account the original statistical error of the lattice results and the uncertainties coming from the matching of the lattice to the continuum theory. A detailed presentation of the relevant formulae at the next-to-leading order and a discussion of the main sources of errors is also presented.
5	9209288	0.002812332006140937	1992-09-28T22:43:01Z	H. Lew, R. R. Volkas,	Discrete quark-lepton symmetry need not pose a cosmological domain wall problem	Quarks and leptons may be related to each other through a spontaneously broken discrete symmetry. Models with acceptable and interesting collider phenomenology have been constructed which incorporate this idea. However, the standard Hot Big Bang model of cosmology is generally considered to eschew spontaneously broken discrete symmetries because they often lead to the formation of unacceptably massive domain walls. We point out that there are a number of plausible quark-lepton symmetric models which do not produce cosmologically troublesome domain walls. We also raise what we think are some interesting questions concerning anomalous discrete symmetries.
6	9308223	0.002778531407906060 4	1993-08-04T15:31:11Z	Michael A. Earnshaw, Margaret James,	Stability of Two Doublet Electroweak Strings	Vortex solutions in the two Higgs doublet electroweak model are constructed, and their stability to small perturbations is studied. The most general perturbation is decomposed into angular momentum modes, the least stable mode is identified, and the linearised energy change of the vortex under this perturbation is calculated numerically for various choices of parameters, thus determining whether or not the string is stable. It is found that, for realistic values of the Higgs mass and Weinberg angle, the string is unstable.
7	9210245	0.002726434479012230 7	1992-10-19T17:49:00Z	O. W. Greenberg,	Scaling limit of a non-relativistic model	I calculate the structure function for scattering from the two-body bound state in its lowest level in a non-relativistic model of confined scalar ``quarks" of masses $m_A$ and $m_B$. The scaling limit in $x={\bf q}^2/2(m_A+m_B)q^0$ exists and is non-vanishing only for the values $x=m_A/(m_A+m_B)$ and $x=m_B/(m_A+m_B)$ which correspond to the fractions of the momentum of the two-body system carried by each of the ``quarks." In the scaling limit, the interference from scattering off of the two ``quarks" vanishes. Thus the scaling limit of this model agrees with the parton picture.
8	9306208	0.002627163169749821	1993-06-02T10:06:11Z	F. R. Klinkhamer,	Existence of a New Instanton in Constrained Yang-Mills-Higgs Theory	Our goal is to discover possible new 4-dimensional euclidean solutions (instantons) in fundamental SU(2) Yang-Mills-Higgs theory, with a constraint added to prevent collapse of the scale. We show that, most likely, there exists one particular new constrained instanton (\Istar) with vanishing Pontryagin index. This is based on a topological argument that involves the construction of a non-contractible loop of 4-dimensional configurations with a certain upperbound on the action, which we establish numerically. We expect \Istar to be the lowest action non-trivial solution in the vacuum sector of the theory. There also exists a related static, but unstable, solution, the new sphaleron \Sstar. Possible applications of \Istar to the electroweak interactions include the asymptotics of perturbation theory and the high-energy behaviour of the total cross-section.
9	9212297	0.002588899471055253 4	1992-12-21T22:14:34Z	L. Durand, K. Honjo, R. Gandhi, I. Sarcevic, H. Pi,	Jets and Jet Multiplicities in High Energy Photon-Nucleon Inelraction	We discuss the theory of jet events in high-energy photon-proton interactions using a model which gives a good description of the data available on total inelastic γp cross sections up to $\sqrt{s}$=210 GeV. We show how to calculate the jet cross sections and jet multiplicities and give predictions for these quantities for energies appropriate for experiments at the HERA ep collider and for very high energy cosmic ray observations.

SBM Community 5

index	arXiv ID	PageRank	Date Published	Author(s)	Title	Summary
0	9207214	0.183926004596714 13	1992-07-04T01:06:35Z	I. I. Bigi, N. G. Uraltsev, A. I. Vainshtein,	Nonperturbative Corrections to Inclusive Beauty and Charm Decays: QCD versus Phenomenological Models	We present a selfconsistent method for treating nonperturbative effects in inclusive nonleptonic and semileptonic decays of heavy flavour hadrons. These effects give rise to powerlike corrections $\propto 1/m_Q^n\,$, $n \ge 2$ with m_Q denoting the heavy quark mass. The leading correction to the semileptonic branching ratio occurs for n=2. It is expressed in terms of the vector-pseudoscalar mass splitting: $\delta BR\ind{sl}/BR\ind{sl} \simeq BR\ind{nl}\, \cdot\,6\,(\,M_V^2-M_P^2)/m_Q^2$ and yields a (\it reduction) of $BR\ind{sl}$. This nonperturbative correction contributes to the nonleptonic width with a sign opposite to that of the perturbative terms that are non-leading in $1/m_c$. In beauty decays the former reduces the latter by 20 \% whereas in charm decays they more or less cancel. This leads to a (\it reduction) of $BR\ind{sl}$ by no more than 10 \% in beauty decays and by a factor of roughly two in charm decays. We confront these results with those obtained from phenomenological models of heavy flavour decays and find that such models are unable to mimic these leading corrections by a specific choice of quark masses or by invoking Fermi motion.
1	9304225	0.144371912552938 8	1993-04-06T22:28:11Z	I. I. Bigi, M. Shifman, N. G. Uraltsev, A. Vainshtein,	QCD Predictions for Lepton Spectra in Inclusive Heavy Flavour Decays	We derive the lepton spectrum in semileptonic beauty decays from a nonperturbative treatment of QCD; it is based on an expansion in $1/m_Q$ with m_Q being the heavy flavour quark mass. The leading corrections arising on the $1/m_Q$ level are completely expressed in terms of the difference in the mass of the heavy hadron and the quark. Nontrivial effects appear in $1/m_Q^2$ terms affecting mainly the endpoint region; they are different for meson and baryon decays as well as for beauty and charm decays.
2	9307247	0.112353924906872 82	1993-07-12T04:08:02Z	B. Blok, L. Koyrakh, M. Shifman, A. I. Vainshtein,	Differential Distributions in Semileptonic Decays of the Heavy Flavors in QCD	Several references added, typos corrected.
3	9308246	0.076536378160255882	1993-08-08T19:07:16Z	Aneesh V. Manohar, Mark B. Wise,	Inclusive Semileptonic B and Polarized Lambda_b Decays from QCD	The differential decay spectrum $d\Gamma/dE_e dq^2$ for the semileptonic decay of an unpolarized hadron containing a b-quark, and the decay spectrum $d\Gamma/dE_e dq^2 d\cos\theta$ for polarized Λ_b decay are computed to second order in the $1/m_b$ expansion. Most of the $1/m_b^2$ corrections have a simple physical interpretation, which is discussed in detail. The implications of the results for the determination of V_{ub} are discussed. The decay spectra for semileptonic decay of hadrons containing a c-quark are also given. There is a subtlety in the use of the equations of motion at order $1/m_b^2$ in the heavy quark expansion which is explained.
4	9308262	0.036008745100379394	1993-08-11T16:01:52Z	Thomas Mannel,	Operator Product Expansion for Inclusive Semileptonic Decays in Heavy Quark Effective Field Theory	Inclusive semileptonic decays are discussed in the framework of heavy quark effective field theory by employing the short distance expansion in the effective theory. The lowest order term turns out to be the parton model, the higher order terms may be regarded as correction terms to the parton model result. The first nonvanishing corrections to the parton model result are given and the lepton energy spectrum of inclusive semileptonic decays of heavy mesons is calculated.
5	9307291	0.020685480179579 76	1993-07-18T14:52:37Z	P. Ball, V. M. Braun,	Next--to--Leading Order Corrections to Meson Masses in the Heavy Quark Effective Theory	We use the QCD sum rule approach to calculate the splitting between vector and pseudoscalar mesons containing one light and one heavy quark, and the kinetic energy of the heavy quark. Our result for the splitting induced by the chromomagnetic interaction agrees to the experimental data on charm and beauty mesons. For the matrix element of the kinetic energy operator, we obtain the value $K=-(0.60\pm 0.10)\, \{\rm GeV\}^2$.
6	9312359	0.020424222259098502	1993-12-31T05:45:29Z	I. I. Bigi, M. A. Shifman, N. G. Uraltsev, A. I. Vainshtein,	On the Motion of Heavy Quarks inside Hadrons: Universal Distributions and Inclusive Decays	In previous papers we have pointed out that there exists a QCD analog of the phenomenological concept of the so called Fermi motion for the heavy quark inside a hadron. Here we show in a more detailed way how this comes about and analyze the limitations of this concept. Non-perturbative as well as perturbative aspects are included. We emphasize both the similarities and the differences to the well-known treatment of deep inelastic lepton-nucleon scattering. We derive a model-independent (\em lower) bound on the kinetic energy of the heavy quark inside the hadron.
7	9311325	0.018037765744961718	1993-11-21T18:55:37Z	Matthias Neubert,	QCD-Based Interpretation of the Lepton Spectrum in Inclusive $\bar B\to X_u\ell\bar\nu$ Decays	We present a QCD-based approach to the endpoint region of the lepton spectrum in $\bar B\to X_u\ell\bar\nu$ decays. We introduce a genuinely nonperturbative form factor, the shape function, which describes the fall-off of the spectrum close to the endpoint. The moments of this function are related to forward scattering matrix elements of local, higher-dimension operators. We find that nonperturbative effects are dominant over a finite region in the lepton energy spectrum, the width of which is related to the kinetic energy of the b-quark inside the B meson. Applications of our method to the extraction of fundamental standard model parameters, among them V_{ub}, are discussed in detail.
8	9401255	0.015892569584285393	1994-01-14T15:04:41Z	C. H. Jin, W. F. Palmer, E. A. Paschos,	A Parton Model for Inclusive Semileptonic B Meson Decays	The parton model for semileptonic B meson decays is studied with special attention to the decay distributions. We find that the spectra show dramatic variations when we introduce cuts on the hadronic energy or invariant mass of hadrons. Results for both $b\rightarrow u$ and $b\rightarrow c$ decays are presented. The detailed spectra may help to separate the two types of decays.
9	9312306	0.015780009179136807	1993-12-20T03:33:07Z	Adam F. Falk, Elizabeth Jenkins, Aneesh V. Manohar, Mark B. Wise,	QCD Corrections and the Endpoint of the Lepton Spectrum in Semileptonic B Decays	Recently, Neubert has suggested that a certain class of nonperturbative corrections dominates the shape of the electron spectrum in the endpoint region of semileptonic B decay. Perturbative QCD corrections are important in the endpoint region. We study the effects of these corrections on Neubert's proposal. The connection between the endpoint of the electron spectrum in semileptonic B decay and the photon spectrum in $b\rightarrow s\gamma$ is outlined.

SBM Community 32

index	arXiv ID	PageRank	Date Published	Author(s)	Title	Summary
0	9207245	0.146594422442296952	1992-07-17T09:48:42Z	Fred Adams, J. R. Bond, Katherine Freese, Joshua Frieman, Angela Olinto,	Natural Inflation: Particle Physics Models, Power Law Spectra for Large Scale Structure, and Constraints from COBE	A pseudo-Nambu-Goldstone boson, with a potential of the form $V(\phi) = \Lambda^4[1 \pm \cos(\phi/f)]$, naturally gives rise to inflation if $f \sim M_{Pl}$ and $\Lambda \sim M_{GUT}$. We show how this can arise in technicolor-like and superstring models, and work out an explicit string example in the context of multiple gaugino condensation models. We study the cosmology of this model in detail, and find that sufficient reheating to ensure that baryogenesis can take place requires $f > 0.3 M_{Pl}$. The primordial density fluctuation spectrum generated is a non-scale-invariant power law, $P(k) \propto k^{n_s}$, with $n_s \simeq 1 - (M^2_{Pl}/8\pi f^2)$, leading to more power on large length scales than the $n_s = 1$ Harrison-Zeldovich spectrum. The standard COBE model with $0 \la n_s \la 0.6-0.7$ could in principle explain the large-scale clustering observed in the APM and IRAS galaxy surveys as well as large-scale flows, but the COBE microwave anisotropy implies such low amplitudes (or high bias factors, $b>2$) for these CDM models that galaxy formation occurs too late to be viable, combining COBE with sufficiently early galaxy formation or the large-scale flows leads to $n_s >0.6$, or $f > 0.3 M_{Pl}$ as well. For extended and power law inflation models, this constraint is even tighter, $n_s > 0.7$, combined with other bounds on large bubbles in extended inflation, this leaves little room for most extended models.
1	9407248	0.133790348559589	1994-07-07T06:55:18Z	Lisa Randall, Scott Thomas,	Solving the Cosmological Moduli Problem with Weak Scale Inflation	Many models of supersymmetry breaking involve particles with weak scale mass and Planck mass suppressed couplings. Coherent production of such particles in the early universe destroys the successful predictions of nucleosynthesis. We show that this problem may be solved by a brief period of weak scale inflation. Furthermore the inflation potential for such an inflation naturally arises from the same assumptions which lead to the cosmological problem. Successful baryogenesis and preservation of density fluctuations for large scale structure formation are also possible in this scenario.
2	9406319	0.111168097656331978	1994-06-15T17:39:45Z	G. Dvali, Q. Shafi, R. Schaefer,	Large Scale Structure and Supersymmetric Inflation without Fine Tuning	We explore constraints on the spectral index n of density fluctuations and the neutrino energy density fraction Ω_{HDM}, employing data from a variety of large scale observations. The best fits occur for $n\approx 1$ and $\Omega_{HDM} \approx 0.15 - 0.30$, over a range of Hubble constants $40-60$ km s^{-1} Mpc^{-1}. We present a new class of inflationary models based on realistic supersymmetric grand unified theories which do not have the usual `fine tuning' problems. The amplitude of primordial density fluctuations, in particular, is found to be proportional to $(M_X /M_P)^2$, where $M_X (M_P)$ denote the GUT (Planck) scale, which is reminiscent of cosmic strings! The spectral index $n = 0.98$, in excellent agreement with the observations provided the dark matter is a mixture of `cold' and `hot' components.
3	9311326	0.098442298639057 6	1993-11-21T21:24:09Z	Hitoshi Murayama, Hiroshi Suzuki, T. Yanagida, Jun'ichi Yokoyama,	Chaotic Inflation and Baryogenesis in Supergravity	We propose a K"ahler potential in supergravity which successfully accommodates chaotic inflation. This model can have a large gravitino mass without giving a large mass to squarks and sleptons, and thus is free from both the gravitino problem and entropy crisis. In this model baryogenesis takes place naturally, identifying the inflaton with a right-handed sneutrino with its mass $M \simeq 10^{13}$GeV, which is consistent with the COBE data and the Mikheyev–Smirnov–Wolfenstein solution to the solar neutrino problem. The model can also accommodate the matter content appropriate for the mixed dark matter scenario.
4	9405389	0.089876732708616 67	1994-05-26T15:00:58Z	Ewan D. Stewart,	Inflation, Supergravity and Superstrings	The positive potential energy required for inflation spontaneously breaks supersymmetry and in general gives any would-be inflaton an effective mass of order the inflationary Hubble parameter thus ruling it out as an inflaton. In this paper we give simple conditions on the superpotential that eliminate the potential sources for this mass, and derive a form for the Kahler potential that eliminates the rest. This reduces the problem of constructing a model of inflation in supergravity to that of constructing one in global supersymmetry with the extra conditions $W=W_\warphi=\psi=0$ during inflation (where W is the superpotential, the inflaton $\in\warphi$, and $W_\psi\neq0$). I then point out that Kahler potentials of the required form often occur in superstrings and that the target space duality symmetries of superstrings often contain R-parities which would make $W=W_\warphi=0$ automatic for $\psi=0$.
5	9503259	0.085830124410526 41	1995-03-07T19:14:23Z	Gia Dvali,	INFLATION VERSUS THE COSMOLOGICAL MODULI PROBLEM	We show that in generic supergravity theories the mass of the moduli during inflation is larger (or at least of the same order of magnitude) than the Hubble constant. This fact does not depends on the details of the inflation and on the value of the Hubble parameter during it. The reason is that inflationary universe is dominated by large F-term (or D-term) density which is higher than the SUSY breaking scale in the present minimum and stabilizes the flat directions of the supersymmetric vacua. Therefore, in general even standard inflationary scenarios (with large H) may solve the cosmological moduli problem.
6	9503303	0.065430274537803 44	1995-03-12T04:57:44Z	Michael Dine, Lisa Randall, Scott Thomas,	Supersymmetry Breaking in the Early Universe	Supersymmetry breaking in the early universe induces scalar soft potentials with curvature of order the Hubble constant. This has a dramatic effect on the coherent production of scalar fields along flat directions. For the moduli problem it generically gives a concrete realization of the problem by determining the field value subsequent to inflation. However it might suggest a solution if the minimum of the induced potential coincides with the true minimum. The induced Hubble scale mass also has important implications for the Affleck-Dine mechanism of baryogenesis. This mechanism requires large squark or slepton expectation values to develop along flat directions in the early universe. This is generally not the case if the induced mass squared is positive, but does occur if it is negative. The resulting baryon to entropy ratio depends mainly on the dimension of the nonrenormalizable operator in the superpotential which stabilizes the flat direction, and the reheat temperature after inflation. Unlike the original scenario, it is possible to obtain an acceptable baryon asymmetry without subsequent entropy releases.
7	9503375	0.050984632713149354	1995-03-18T16:49:41Z	Gia Dvali,	INFLATION INDUCED SUSY BREAKING AND FLAT VACUUM DIRECTIONS	We discuss how the inflation induced supersymmetry breaking affects the flat directions of SUSY vacua. We show that under general assumptions all gauge nonsinglet fields, parameterizing flat directions (and in particular squarks and sleptons), get large $radiative$ masses which are related to the value of the Hubble constant (H) and to the expectation value of the inflaton field. This mass (typically $\sim H$) is of ``non-gravitational" origin and does not vanishes in the global SUSY limit. Large radiative corrections are induced by F-term (or D-term) density, which dominates the inflationary universe and strongly breaks supersymmetry. In such theories it is difficult to treat squarks and sleptons as the light fields in the inflationary period. In the generic supergravity theories all flat directions, including moduli, are getting curvature of order the Hubble constant. However, for the gauge-nonsinglet flat directions radiative contribution to the curvature (induced by renormalizable gauge interactions) may be dominant.
8	9504420	0.043576613666393677	1995-04-28T03:30:42Z	Tony Gherghetta, Gordon L. Kane,	Chaotic inflation and a radiatively generated intermediate scale in the supersymmetric standard model	We consider a phenomenological extension of the minimal supersymmetric standard model which incorporates chaotic inflation and a radiatively generated intermediate mass scale. Initially a period of chaotic inflation is driven by a quartic potential associated with the right-handed electron sneutrino. Supersymmetry relates the quartic coupling of the inflationary potential to the electron Majorana neutrino Yukawa coupling, h_1. The microwave background temperature anisotropy determines this coupling to be $h_1\simeq 10^{-7}$, which is similar in magnitude to the electron Dirac Yukawa coupling. A U(1) Peccei-Quinn (PQ) symmetry is broken by radiative corrections at an intermediate scale $\simeq 10^{12}$GeV when the universe cools to a temperature $T\lesssim 10^3$GeV. This leads to an invisible axion, a weak scale μ-term and an electron Majorana neutrino mass $M_{N_1}\simeq 10^5$GeV. A second inflationary period can also occur via a flat-direction field. In this case the universe can be reheated to a temperature $T_{RH}\simeq 10^6$GeV, without restoring PQ symmetry. Baryogenesis will then occur via out-of-equilibrium neutrino decay.
9	9502417	0.043576613666393677	1995-02-28T21:13:26Z	David H. Lyth, Ewan D. Stewart,	Cosmology with a TeV mass GUT Higgs	The most natural way to break the GUT gauge symmetry is with a Higgs field whose vacuum expectation value is of order $10^{16}\,\mbox{GeV}$ but whose mass is of order 10^2 to $10^3\,\mbox{GeV}$. This can lead to a cosmological history radically different from what is usually assumed to have occurred between the standard inflationary and nucleosynthesis epochs, which may solve the gravitino and Polonyi/moduli problems in a natural way.

SBM Community 34

index	arXiv ID	PageRank	Date Published	Author(s)	Title	Summary
0	9306289	0.17224047463628417	1993-06-18T16:50:00Z	F. E. Close, R. G. Roberts,	Consistent Analysis of the Spin Content of the Nucleon	The recent measurements of lepton nucleon scattering with polarised neutron and deuteron targets are analysed together with the previous polarised proton data in a mutually consistent way. The detailed x-dependence of the polarisation asymmetry in the valence region is shown to be in agreement with historical predictions based on quark models. The Bjorken sum rule is shown to be confirmed at the 1σ level and estimates of the spin content of the nucleon Δq are extracted. While the average value of Δq from the three experiments comes out to be 0.41 ± 0.05 (to be compared with the naive quark model theoretical expectation of 0.58) this experimental average value is more than one standard deviation from the value obtained from any individual experiment.This inconsistency can be overcome by allowing arbitrary higher twist contributions but the resulting precision is poor, $\Delta q = 0.38\pm 0.48$.
1	9404270	0.10435816100868865	1994-04-15T08:56:12Z	the SMC,	Measurement of the Spin-Dependent Structure Function $g_1(x)$ of the Proton	We have measured the spin-dependent structure function g_1^p of the proton in deep inelastic scattering of polarized muons off polarized protons, in the kinematic range $0.003<x<0.7$ and $1\,\mbox{GeV}^2<Q^2<60\,\mbox{GeV}^2$. Its first moment, $\int_0^1 g_1^p(x) dx $, is found to be $0.136 \pm 0.011\,(\mbox{stat.})\pm 0.011\,(\mbox{syst.})$ at $Q^2=10\,\mbox{GeV}^2$. This value is smaller than the prediction of the Ellis--Jaffe sum rule by two standard deviations, and is consistent with previous measurements. A combined analysis of all available proton, deuteron and neutron data confirms the Bjorken sum rule to within 10% of the theoretical value.
2	9305306	0.10290294672256806	1993-05-24T14:18:31Z	John Ellis, Marek Karliner,	Analysis of Data on Polarized Lepton-Nucleon Scattering	We re-analyze data on deep inelastic polarized lepton-nucleon scattering, with particular attention to testing the Bjorken sum rule and estimating the quark contributions to the nucleon spin. Since only structure function data at fixed Q^2 can be used to test sum rules, we use E142 asymmetry measurements and unpolarized structure function data to extract g_1^n at fixed Q^2 = 2 GeV^2. When higher-twist effects, which are important at low Q^2, are included, both the E142 and SMC data are compatible with the Bjorken sum rule within one standard deviation. Assuming validity of the Bjorken sum rule, we estimate the quark contributions to the nucleon spin, finding that their total net contribution is small, with the strange quark contribution non-zero and negative. The quark spin content of the nucleon spin is in agreement with Skyrme model.
3	9311255	0.07114986299617793	1993-11-10T08:41:00Z	G. Altarelli, P. Nason, G. Ridolfi,	On the Q^2 Dependence of Measured Polarized Structure Funtions	We analyse the available data on the polarized asymmetries A_1 for proton, neutron and deuteron targets. We use a homogeneous and updated set of unpolarized structure functions to derive g_1 from A_1, and we accurately correct for the scaling violations in order to obtain $g_1(x,Q^2)$ with the same Q^2 for all x values. The contribution to the Q^2 evolution of a possible large gluon polarized density is also considered. The implications for the Ellis-Jaffe and for the Bjorken sum rules are discussed.
4	9310272	0.027151465306968846	1993-10-12T16:06:00Z	John Ellis, Marek Karliner,	Spin Structure Functions	We review the theory and phenomenology of deep inelastic polarized lepton-nucleon scattering in the light of recent data with a deuteron target from the SMC at CERN and a Helium 3 target from the E142 experiment at SLAC. After including higher-order perturbative QCD corrections, mass corrections and updated estimates of higher-twist effects, we find good agreement with the basic Bjorken sum rule, and extract a consistent set of values for the quark contributions to the proton spin: $$\Delta\Sigma \equiv \Delta u + \Delta d + \Delta s = 0.27 \pm 0.11 $$ $$\Delta u = 0.82 \pm 0.04, \Delta d = -0.44 \pm 0.04,\Delta s = -0.11 \pm 0.04 $$ which are consistent with chiral soliton models and indications from lattice estimates. We also mention the prospects for future experiments on the spin structure of the nucleon.
5	9305322	0.02349789989409829	1993-05-26T14:59:10Z	S. D. Bass, A. W. Thomas,	Mapping the x dependence of the axial anomaly in polarised deep inelastic scattering	We discuss the role of the U(1) axial anomaly in the spin structure functions of the nucleon, with particular emphasis on how one might determine its x dependence in present and future deep inelastic scattering experiments. We focus on the C-odd spin structure function g3 and also the deuteron structure function g1^d.
6	9311285	0.023241637000409328	1993-11-12T15:59:03Z	B. Ehrnsperger, L. Mankiewicz, A. Schäfer,	OPE analysis for polarized deep inelastic scattering	We present an explicit OPE analysis for the first moment of g_1 up to order M^2/Q^2. This result allows to calculate power corrections to the Bjorken and Ellis--Jaffe sum rules.
7	9310306	0.02274641633558571 4	1993-10-18T15:19:20Z	S. D. Bass, A. W. Thomas,	The Spin Structure of the Nucleon	We provide an introduction to the ideas of spin-dependent deep-inelastic scattering. Recent experimental results are summarised and possible explanations related to the axial anomaly presented. Further experiments that could greatly clarify the situation are also described.
8	9403383	0.02203697919493376	1994-03-29T08:09:31Z	S. A. Larin,	The next-to-leading QCD approximation to the Ellis-Jaffe sum rule	The \alpha_s^2 correction to the Ellis-Jaffe sum rule for the structure function g_1 of polarized deep inelastic lepton-nucleon scattering is calculated.
9	9305323	0.02108413152471595 4	1993-05-26T15:07:42Z	S. D. Bass,	Gauge symmetry and the EMC spin effect	We emphasise the EMC spin effect as a problem of symmetry and discuss the renormalisation of the $C=+1$ axial tensor operators. This involves the generalisation of the Adler-Bell-Jackiw anomaly to each of these operators. We find that the contribution of the axial anomaly to the spin-dependent structure function $g_1 (x, Q^2)$ scales at $O(\alpha_s)$. This means that the anomaly can be a large x effect in g_1. Finally we discuss the jet signature of the anomaly.

As we see above, all of the Label Propagation and SBM communities' top papers are on the **same or similar subjects**, indicating **very good** community detection. However, we were **unable** to find similarity in the top Louvain communities' papers, indicating **poor** community detection.

Louvain was **unable** to discern between small and medium communities and found large communities with **high** modularity but **poor** paper similarity.

To understand this further, we draw the condensation graph for each algorithm at different time slices. The condensation graph is a graph where each node denotes a community and links between nodes indicates a link between nodes belonging to those communities. We plot them for time slices 0,15, and 29.

Label Propagation Snapshot 0

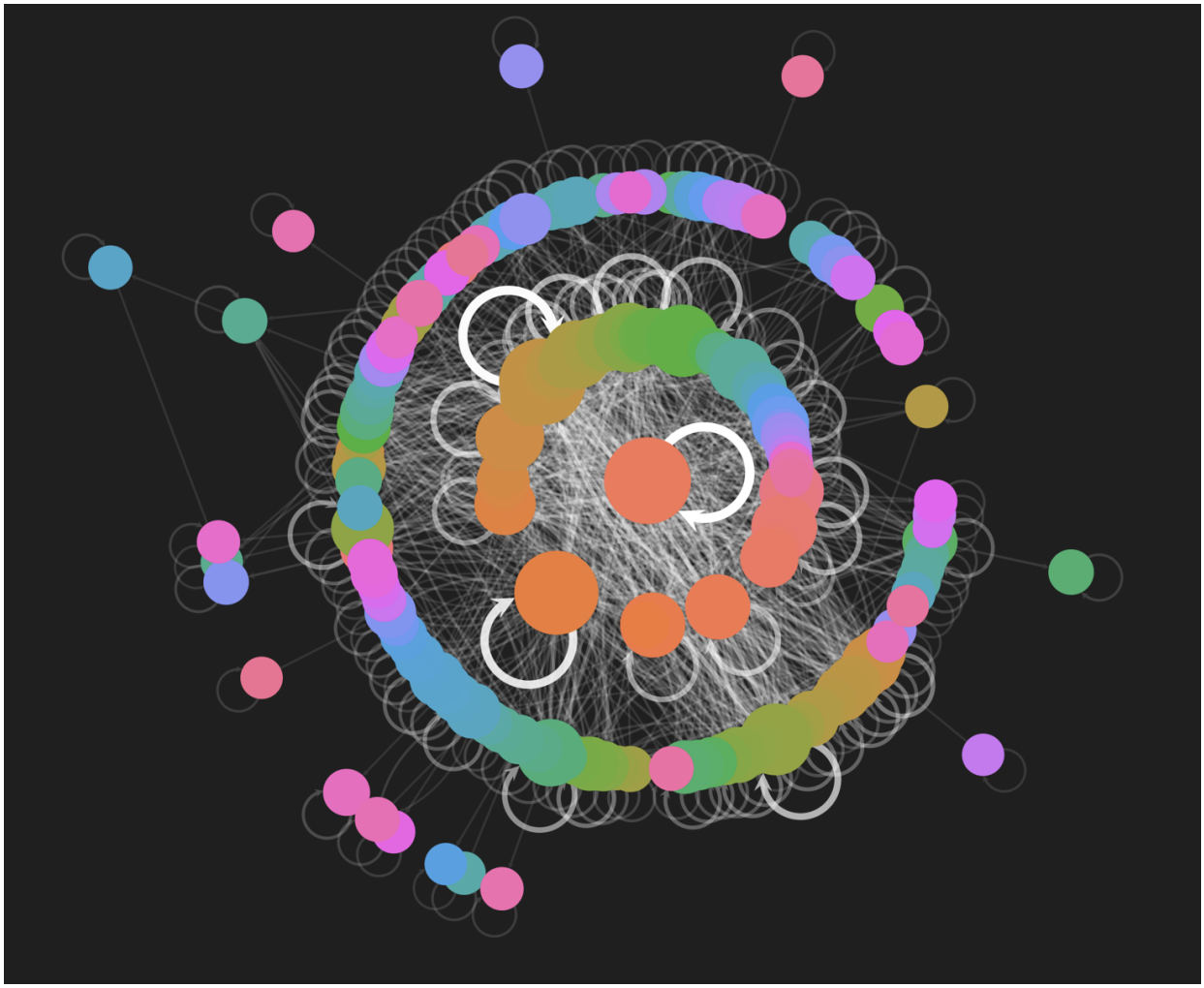

Label Propagation Snapshot 15

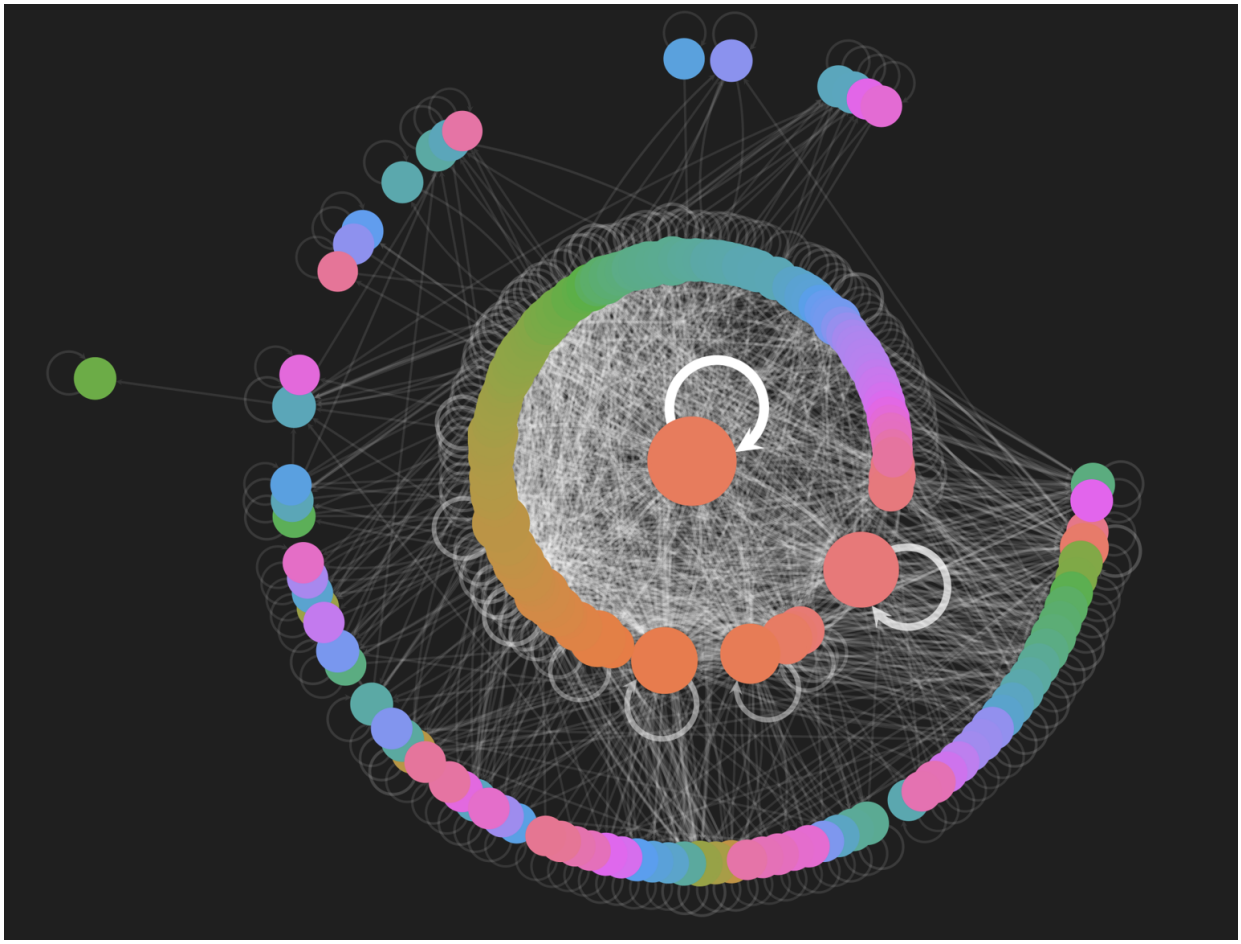

Label Propagation Snapshot 29

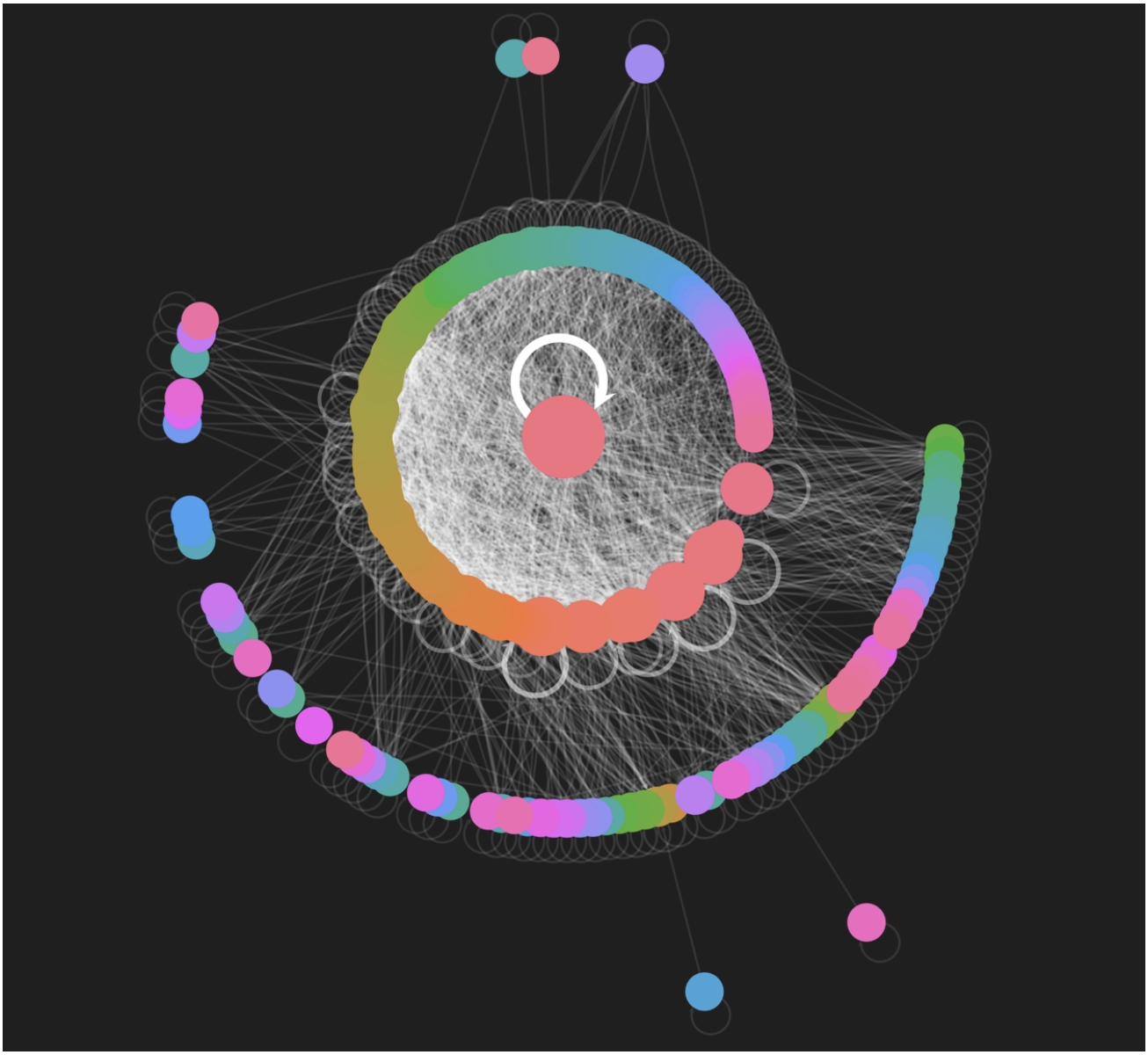

Louvain Snapshot 0

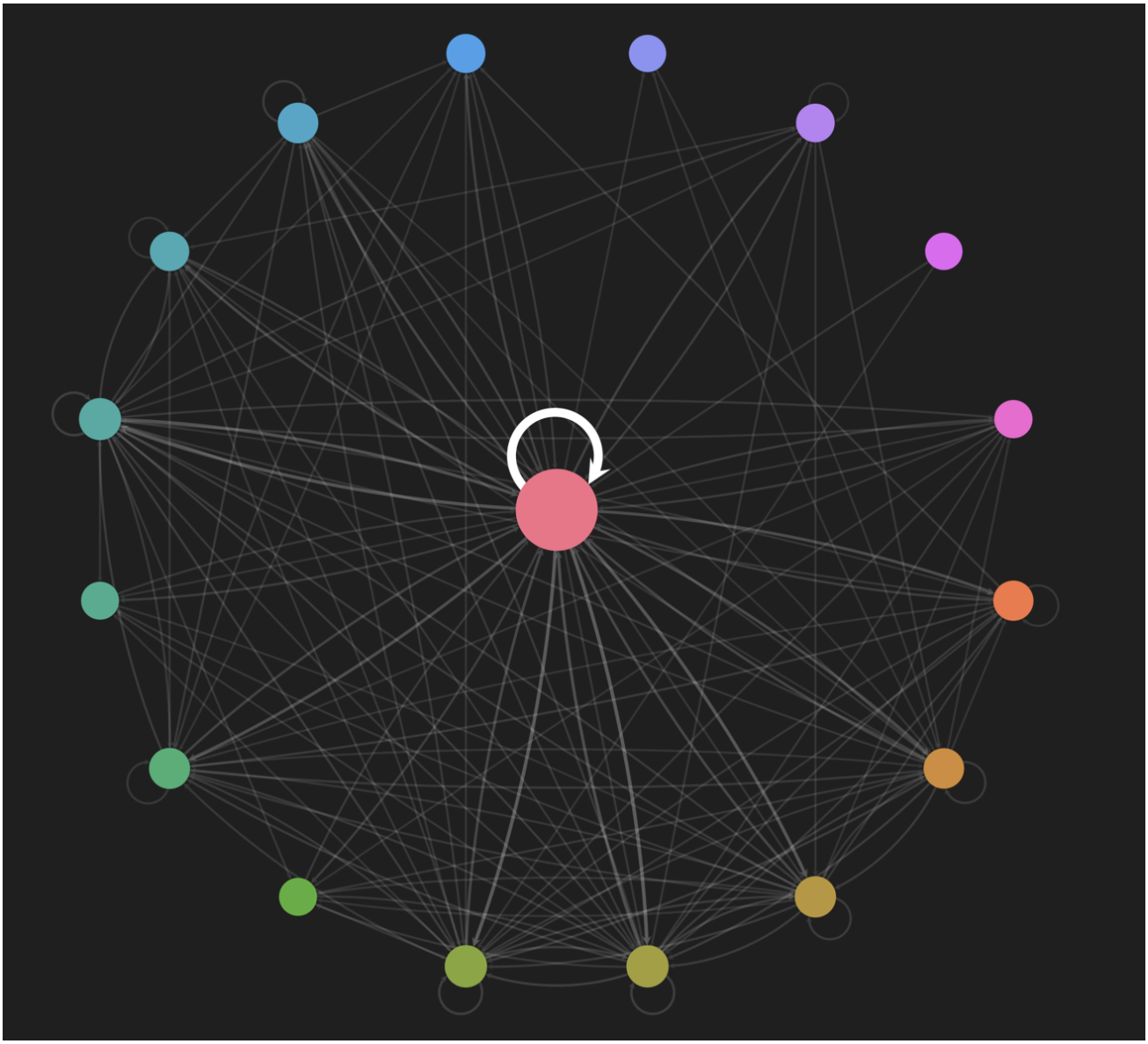

Louvain Snapshot 15

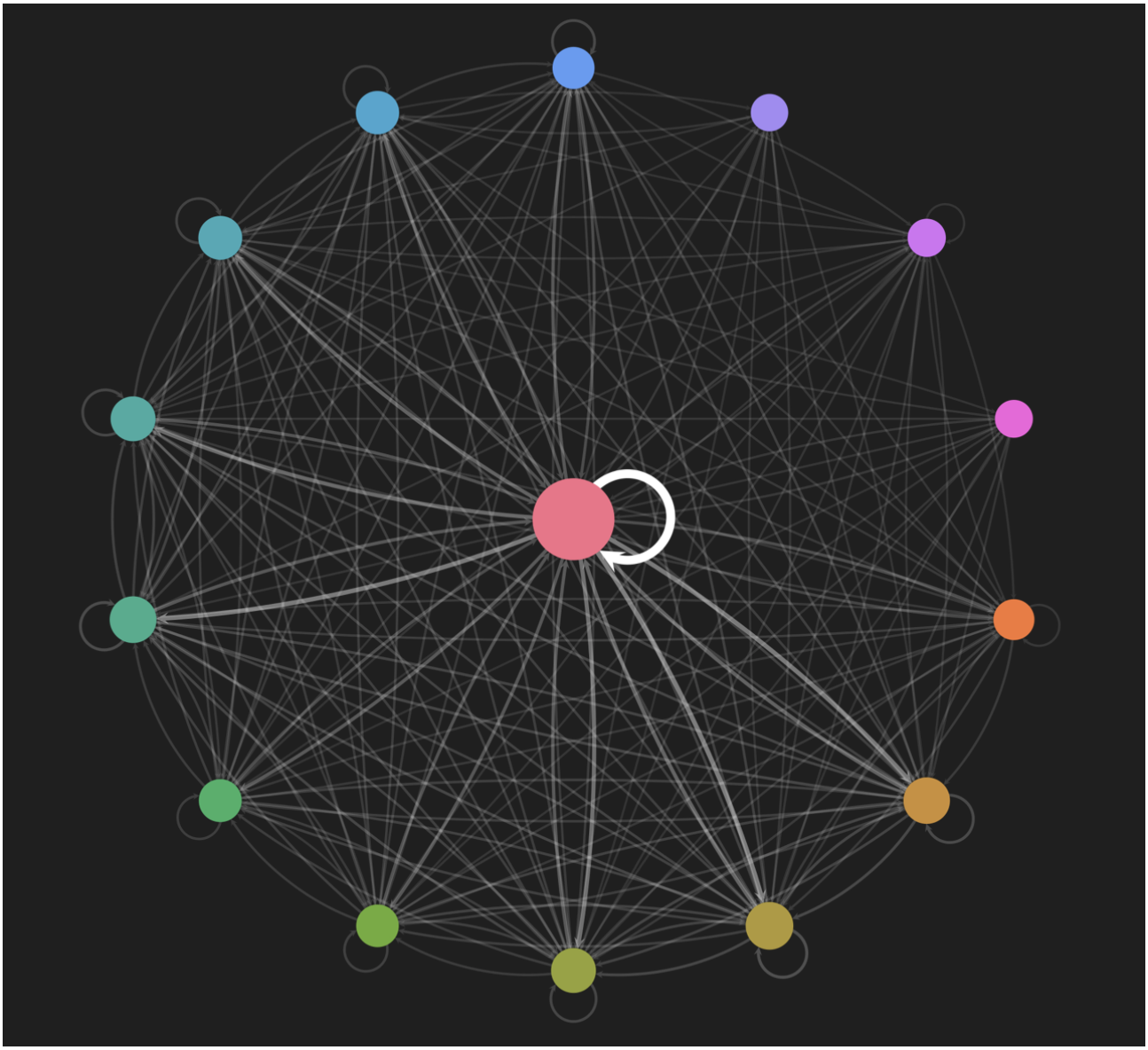

Louvain Snapshot 29

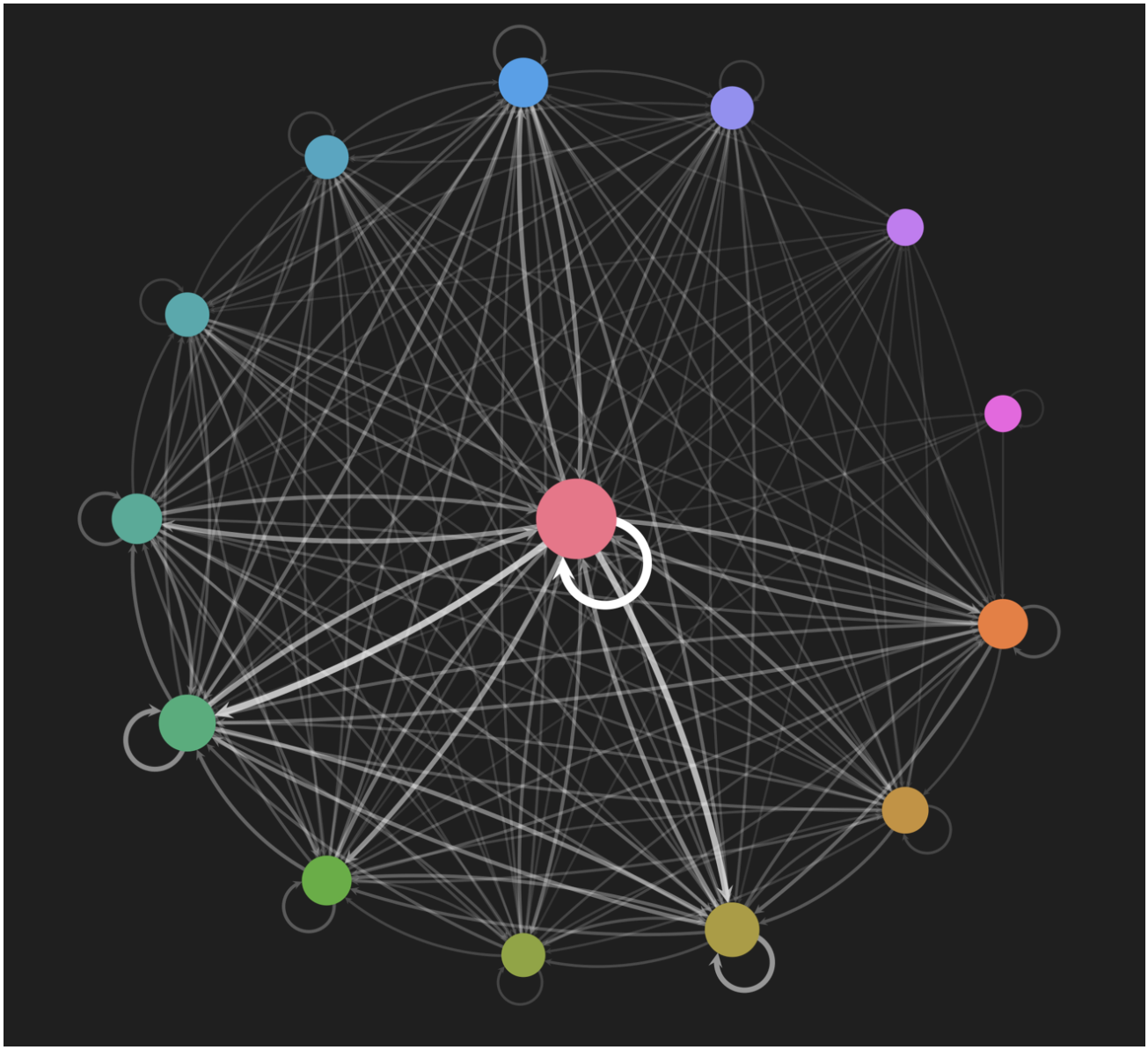

SBM Snapshot 0

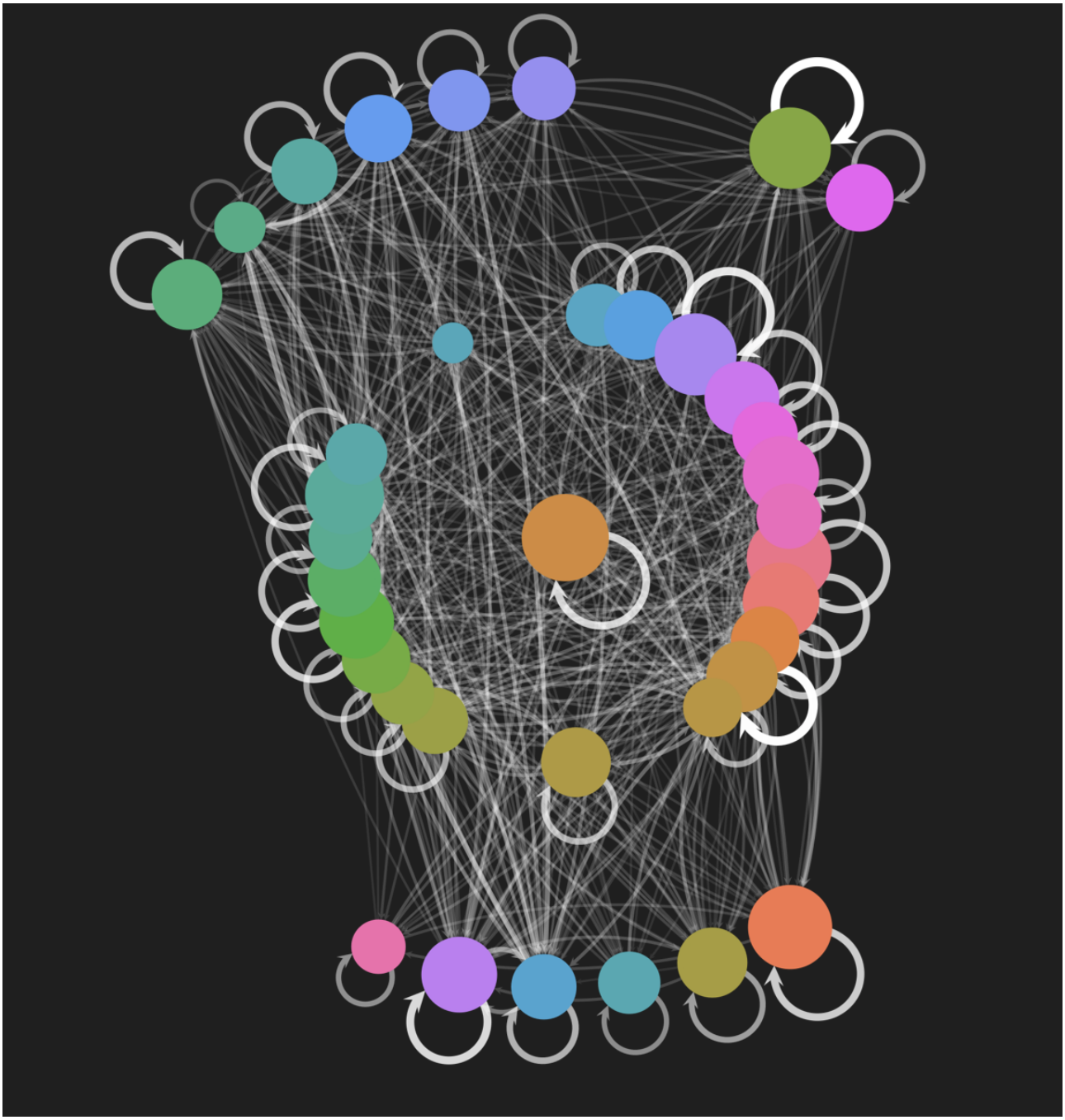

SBM Snapshot 15

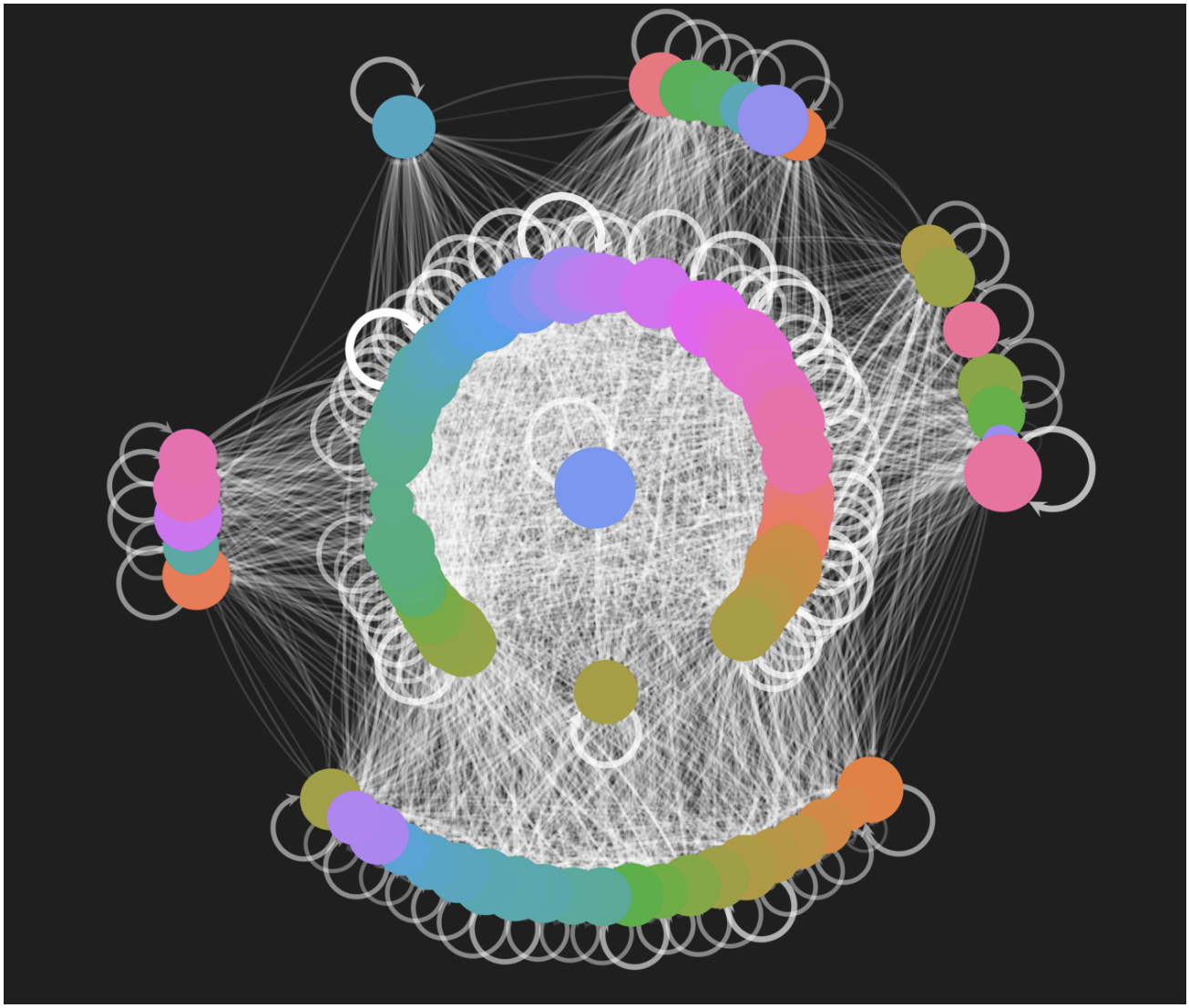

SBM Snapshot 29

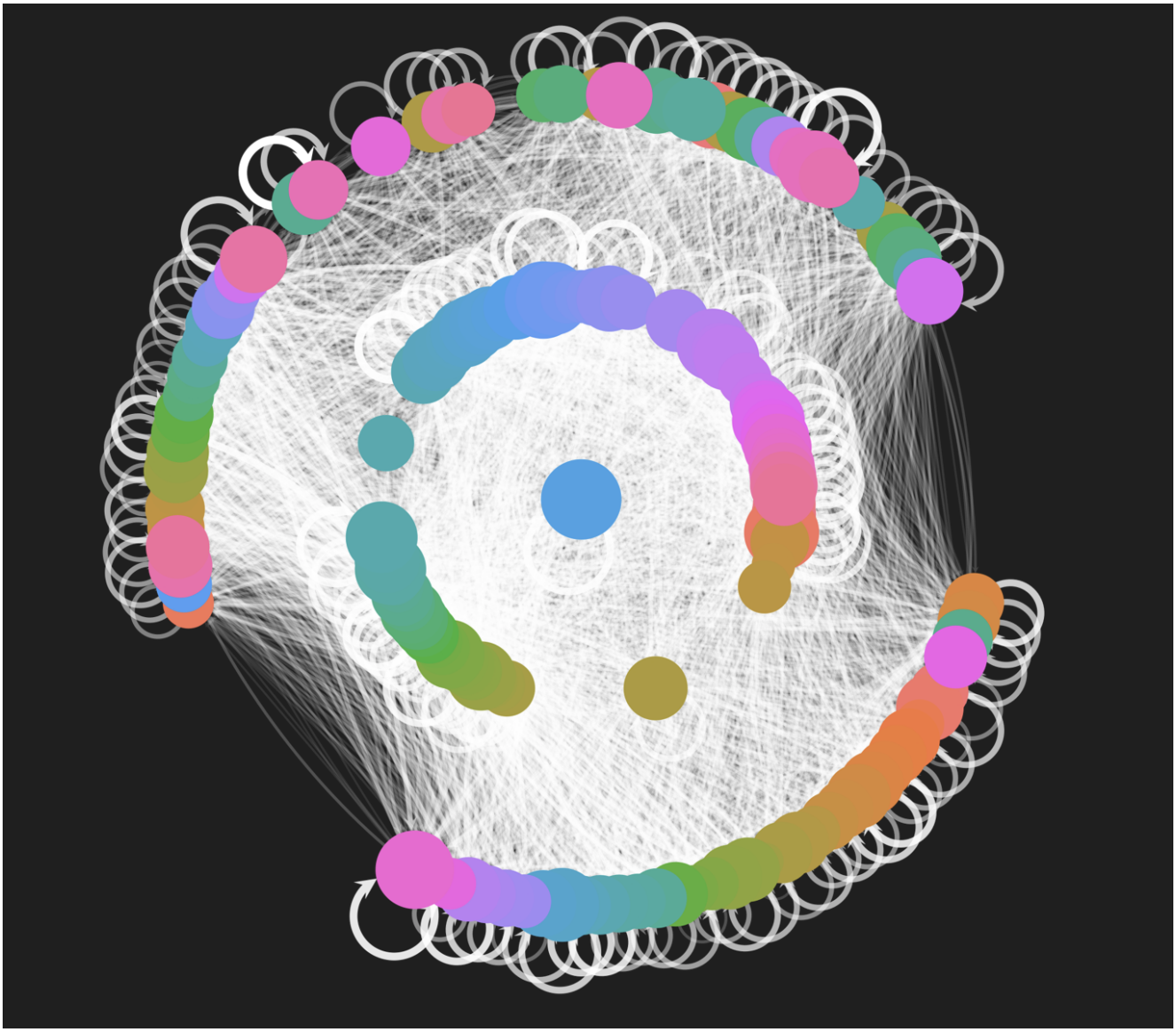

As we can see above, Label Propagation has one large community but also has **several** well connected medium sized communities of good quality (We define good quality here by looking at the self loops. We see that the self-loops are quite large and there is good **interconnectivity** between communities) and the medium sized communities get smaller over time compared to the large community. This doesn't mean the medium sized communities reduce in quality, but rather that they the large community grows larger and larger relative to these communities. The medium sized communities stay quite large and well connected.

SBM has **several** well connected medium sized communities of good quality throughout the snapshots. The communities are **highly** interconnected and are at the same time highly **intra-connected**. This makes sense in the context of sub-fields of a research area. The sub-fields would all have high **intra-connectivity** as they borrow from other papers in their own sub-field, but they would also have high **interconnectivity** as they would also rely upon research in other sub-fields for some parts of their paper.

Louvain has **terrible** small communities of **very poor** quality, and a massive highly intra-connected community linked to these small communities. We cannot say that this large

community has good quality as it is so large, it quite obviously would have high intra-connectivity. Louvain merely maximizes modularity without caring about **network structure**. Both Label Propagation and SBM rely heavily upon the underlying network structure to make community predictions.

Summary And Takeaways

Through our analysis, we come out with a few takeaways -

- The addition of temporal data to a citation network improves the Label Propagation and the SBM results, resulting in good community structure throughout the snapshots.
- Conductance was quite good for Label Propagation and Louvain. Further analysis may be necessary to see whether SBM continues to plateau or instead increases again as network size increases.
- Louvain, albeit a good algorithm for some graphs, is not the winner when it comes to finding communities in temporal networks. Perhaps its predecessor, the Leiden algorithm, may work better here in finding communities. If not, perhaps modularity is not the best measure of a good partition of the network.
- Label Propagation, an extremely fast algorithm, works well when finding communities in temporal networks due to its reliance on the underlying network structure. Further analysis may be necessary to see whether this is occurring due to the structure of this specific network, or Label Propagation is itself good.
- SBM inferencing, a relatively recent method, works well when finding communities in temporal networks. It works well and provides consistent results throughout all snapshots.
- Our analysis of the arXiv API data was limited due to time constraints and hence was limited to only the communities with the largest consistent community sizes. Perhaps further analysis of this data would lead to more interesting conclusions on the accuracy of SBM and Label Propagation.
- My implementation of Louvain *may* be flawed, causing it to focus on large communities to improve modularity. At the end of temporal analysis, the partition found by Louvain had a modularity of 0.59, which was lower than when we statically calculated it on the full graph. This may be due to the fact that the final snapshot is prior to the date cutoff of the full graph, but further analysis would be necessary to conclude so. The modularity is still quite high in the context of such large networks.

- Our results may be affected by the fact that this network is getting **denser** over time. Perhaps results on a network that gets **sparser** over time may reveal completely different results.

Source Code

The source code, plots, and data are present at https://github.com/notrudyyy/arXiv-Hep-Ph-Analysis

References

[1] - https://snap.stanford.edu/data/cit-HepPh.html

[2] - https://graph-tool.skewed.de/

[3] - https://arxiv.org/pdf/cs/0309023.pdf

[4] - https://arxiv.org/pdf/1503.05641.pdf

[5] - https://www.cs.cmu.edu/~jure/pubs/powergrowth-kdd05.pdf